PRELIMINARY STUDY OF TRIBOLOGY: UNIFORM CONTROL OF

THE DENSITY CONTROL OF THE FUNCTIONALIZED GOLD

NANOPARTICLES ON A MODIFIED SILICON SURFACE

Except where reference is made to the work of others, the work described in this thesis is
my own or was done in collaboration with my advisory committee. This thesis does not
include proprietary or classified information.

_____
Chan-kyu Kang

Certificate of Approval:

_____   _____
Christopher B. Roberts   W. Robert Ashurst, Chair
Professor   Assistant Professor
Chemical Engineering   Chemical Engineering

_____   _____
Mario R. Eden   Joe F. Pittman
Assistant Professor   Interim Dean
Chemical Engineering   Graduate School

PRELIMINARY STUDY OF TRIBOLOGY: UNIFORM CONTROL OF

THE DENSITY CONTROL OF THE FUNCTIONALIZED GOLD

NANOPARTICLES ON A MODIFIED SILICON SURFACE

Chan-kyu Kang

A Thesis

Submitted to

the Graduate Faculty of

Auburn University

in Partial Fulfillment of the

Requirements for the

Degree of

Master of Science

Auburn, AL
May 10, 2007

PRELIMINARY STUDY OF TRIBOLOGY: UNIFORM CONTROL OF

THE DENSITY CONTROL OF THE FUNCTIONALIZED GOLD

NANOPARTICLES ON A MODIFIED SILICON SURFACE

Chan-kyu Kang

_____

Signature of Author

_____

Date of Graduation

VITA

Chan-kyu Kang was born on September 13, 1975, in Sangju, Republic of Korea. He was graduated from the Chemical Engineering Department at Yeungnam University with a Bachelor of Science degree in 2001. He then worked at Doosan Electro-Material Company as a quality assurance engineer. He attended the master's degree program in Chemical Engineering at Lamar University and received the degree of Master of Science in August 2001. His research at Lamar University was on air pollution measurement and simulation. He entered Graduate School at Auburn University, in August, 2004 where he worked under the supervision of Dr. W. Robert Ashurst.

THESIS ABSTRACT

PRELIMINARY STUDY OF TRIBOLOGY: UNIFORM CONTROL OF

THE DENSITY CONTROL OF THE FUNCTIONALIZED GOLD

NANOPARTICLES ON A MODIFIED SILICON SURFACE

Chan-kyu Kang

Master of Science, May 10, 2007
(M. S., Lamar University, 2003)
(B. S., Yeungnam University, 2001)

89 Typed Pages

Directed by W. Robert Ashurst

Microelectromechanical Systems (MEMS) are important in diverse fields such as BioMEMS, optical MEMS, and radio frequency MEMS. The low cost, small device size and high reliability are contributing to successful commercialization in MEMS markets. However, the miniature device components can generate surface forces that form undesirable tribological issues between microstructures. The important interfacial forces are capillary, molecular Van der Waals forces and electrostatic force. The uniform distribution of gold nanoparticles can be used to study tribological issues in MEMS devices. Simple methods to control the density control of colloidal gold nanoparticles on silicon surfaces were investigated. Preliminary work showed that and silicon surfaces modified with 3-MPTMS solution interact with gold nanoparticles. Atomic force

microscopy (AFM) images support the notion that Si surface modification is the most important work in this study with ligand modified gold nanoparticles. The examination of the density control on a silicon surface can be manipulated through control of the concentration of colloidal gold nanoparticles, deposition time, concentration of 3-MPTMS solution, and temperature. A relatively high density of gold nanoparticles forms on the silicon surface if the concentration of gold nanoparticles and 3-MPTMS is increased. In addition, with a 3 hour deposition time we find a maximum number of gold nanoparticles while thermal effects are minimal. However, there are some restrictions on experimental conditions because it is not possible to control gold nanoparticles density on a dirty surface. Mathematical equations used with the particle analysis tool in AFM take advantage of the expected the particle density.

ACKNOWLEDGMENTS

The author would like to express his utmost gratitude to his advisor, Dr. W. Robert Ashurst, for always providing the patient guidance and an atmosphere of respect that made this work possible. The author also expresses his gratitude to the other members of his advisory committee, Dr. Christopher B. Roberts and Dr. Mario R. Eden.

The author's appreciation from the bottom of his heart also goes to Dr. Jae-Jin Shim, Dr. Tae-Hoon Kim, Miss. Dorothy and my family for giving me an opportunity to pursue higher education and their valuable advices.

Thanks are also due to his wife, Sang-Mi Lee, for her unwavering love and encouragement.

Style manual or journal used THE ACS STYLE GUIDE: A MANUAL FOR AUTHORS

AND EDITORS

Computer software used MICROSOFT WORD 2003

TABLE OF CONTENTS

LIST OF TABLES

LIST OF FIGURES

CHAPTER 1

INTRODUCTION OF MEMS

1.1 Definition of Microelectromechanical Systems (MEMS)

Microelectromechanical systems (MEMS) are an assembly of sensors, actuators, and mechanical elements on silicon wafers. However, the definition of MEMS continues to evolve beyond this traditional definition because they are now being applied to widely diverse fields such as BioMEMS, optical MEMS, and radio frequency MEMS. In Europe, MEMS are called Micro Systems Technology (MST), while in Japan they are referred to as Micromachines [1]. As the MEMS technology allows the assembly of smaller elements, it now also includes Nanoelectromechanical Systems (NEMS). Despite the various advantages of such devices, fabrication techniques are not available because of insufficient physical prototypes to allow valid simulations [2]. Figure 1-1 shows MEMS products from Sandia National Laboratories.

The origin of MEMS technology is rooted in the discovery of semiconductors at Bell Laboratories in the early 1950s. In the beginning of the 1990s, MEMS were used to aid of the development of the integrated circuit (IC) fabrication process. MEMS devices began to enter the marketplace in the mid-1990s and bulk micromachining, surface micromachining, and LIGA processes were used for MEMS fabrication by the end of the 1990s. Commercial MEMS devices include pressure, temperature, chemical and vibration sensors, light reflectors, accelerometers for airbags, and vehicle controls. MEMS devices

have also been used to move fluids (gases and liquids) to amplify and identify strands of DNA, and carry out biochemical analysis of very small quantities of materials [3].
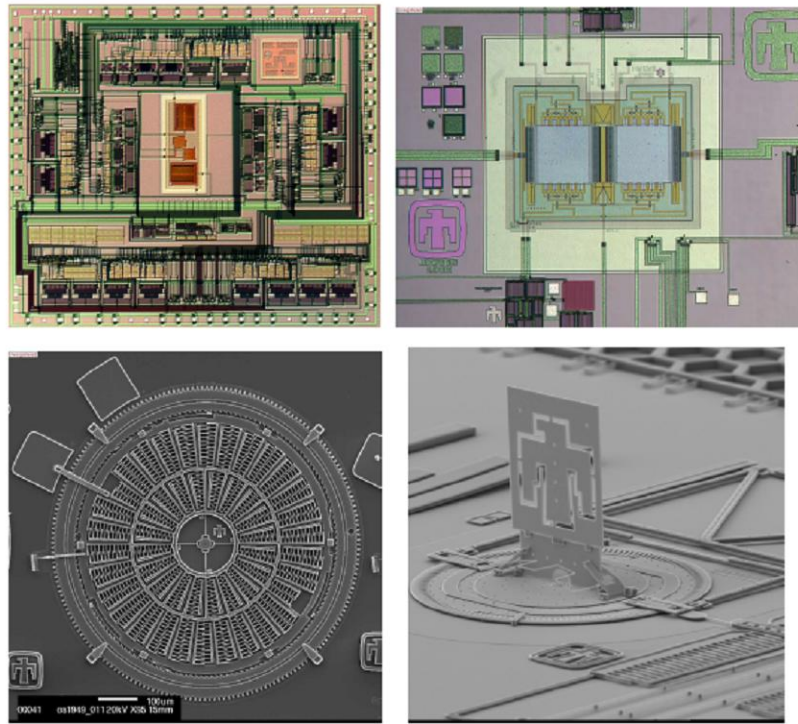
Figure 1-1 *Various MEMS products from Sandia National Laboratory*

The core elements in MEMS are composed of sensors and actuators [4]. The consideration of actuator design is deeply influenced by the fact that two moving parts or a moving and a fixed part make physical contact in a MEMS device. This phenomenon is known as tribology, a term derived from the Greek word tribo (to rub), which is defined as the science and technology of interacting surfaces with respect to relative motion. It encompasses friction, wear and lubrication. It is important for MEMS because tiny mechanical devices are built on silicon or silicon-related materials with mature fabrication technologies and unique properties [5].

Silicon is the most widely used substrate material because it is extremely flat, easy to fabricate, and allows chemical coating. However, silicon materials have their shortcomings. The polycrystalline silicon surface rapidly oxidizes with air to form a hydrophilic oxide layer, and this layer can be quite thick depending on processing conditions [6]. In addition, the friction, adhesion, and wear behavior properties of silicon have drawbacks, so there have been attempts to develop new materials to replace silicon [7]. Currently, polymers are beginning to be used in the field of bio-MEMS and microfluidic devices because of their resistance to corrosion and flexibility [5]. In addition, research and development in MEMS materials is useful in textile industry (textile MEMS).

Since the term MEMS evolved in the United States in the 1990s, MEMS technology has received a lot of attention from the public and private sectors [1]. The potential impact of the MEMS industry on US businesses is immense:

• The US market for MEMS is projected to increase to just over 19 percent per annum through 2008 to $3.3 billion.

• MEMS were nominated by Business Week as one of the three technologies expected to future growing technologies.

• The widest application of MEMS includes air bag accelerometers, ink-jet printer heads and blood pressure monitors, and new applications will expand the use of MEMS.

Also, several technical factors contributed to the expanding MEMS industry:

• easy access to ultra-pure (no mechanical fatigue), low cost materials

• sophisticated diagnostic and testing equipment.

• high-volume IC (integrated circuit) packaging technologies.

3

• low-cost and high-volume batch wafer processing technology.

1.2 MEMS Fabrication Techniques

Silicon micromachining is an important factor for the development of MEMS technology. The three major MEMS fabrication techniques are bulk micromachining, surface micromachining, and the LIGA process. Figure 1-2 and 1-3 show various steps of these three techniques. Bulk and surface micromachining use planar photolithographic fabrication processes to produce two-dimensional structures [8, 9] and those two techniques are widely adapted for MEMS and Microsystems manufacturing. The LIGA process has been used for 3D microstructure fabrication and allows on-demand manufacture of high-aspect- ratio structure [10].

1.2.1 Bulk micromachining

Bulk micromachining produces structures inside silicon substrates. This technique was first used in microelectronics in the 1960s, and it evolved to allow production of three-dimensional microstructures in the 1970s. The major commercial devices that are made using bulk micromachining techniques include pressure sensors, silicon valves, and silicon accelerometers. Bulk micromachining allows the selective removal of silicon from a substrate to make a variety of structures and takes advantage of all three dimensions of space (x, y, and z). This technique is analogous to that used by a sculptor, who creates shapes out of large unformed materials. In this case, the structural material is removed by physical or chemical means. Bulk micromachining is divided into wet etching and dry etching, which depends upon the phase of etchant. The most common etch in silicon is

anisotropic wet etching. Liquid etchants are used to produce wet etching, while vapor and plasma etchants are used to produce dry etching. Anisotropic etching is the key technology for removal of sections of material ranging from 250 to 500 μm thick [11, 12]. Isotropic etching is also called orientation-independent etching. Isotropic etching has drawbacks in that it is difficult to control the final geometry of the surface structure and most substrate materials do not have an isotropic crystalline structure. Figure 1-2 shows an example of the bulk micromachining process. The process begins with a silicon wafer. Thermal oxide layers are existed on both side of the wafer (Figure 1-2a). The photoresist is then photolithographically patterned and developed. With using hydrofluoric acid solutions, the pattern in the photoresist is transferred into the oxide layer (Figure 1-2b). The photoresist is selectively dissolved in the acetone. The oxide layer serves as a mask during a wet anisotropic etching (Figure 1-2c). This structure consist of a bottom {100} plane and {111} side walls. Strain sensors are deposited on strategic locations of membrane by means of depositing and patterning doped polycrystalline silicon (Figure 1-2d). The part of substrate that is not covered by the protective mask is dissolved in the etchants and removed in the second step.
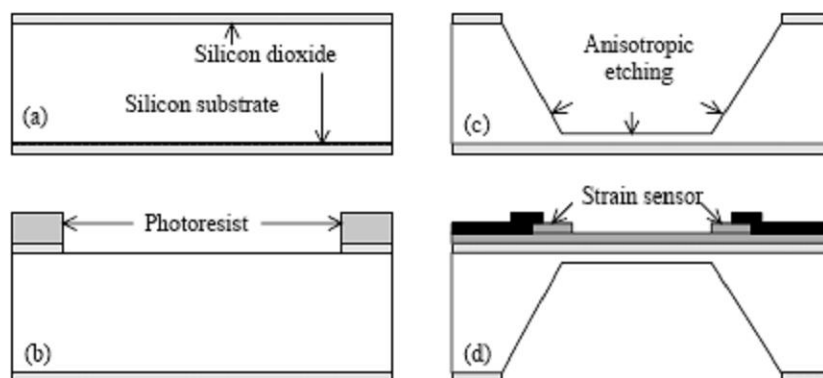
Figure 1-2 Bulk micromachining process

1.2.2 Surface micromachining

In contrast to bulk micromachining, surface micromachining is the fabrication of micromechanical structures by deposition and etching of a thin structure and a sacrificial layer on top of a silicon substrate. Polycrystalline silicon (polysilicon) is a common layer material. In MEMS, silicon dioxide is used as the sacrificial layers in the construction of complicated components like movable parts, but is removed later to create the void spaces necessary to create the appropriate depth [4]. Low-pressure chemical vapor deposition techniques (LPCVD) are commonly used for building up the components while wet etching is the common method used to create void spaces. Factors to consider during surface micromachining are (1) the proper structural material, (2) good mechanical properties of the sacrificial material, and (3) excellent selective of the chemical etchant. Figure 1-3 shows a surface micromachining processing sequence using polysilicon and silicon dioxide. Deposition and patterning of the sacrificial layer is performed in step 1. Deposition and patterning of the polysilicon microstructure layer is performed in step 2. The sacrificial layer is etched away to produce the freestanding cantilever beam in step 3.
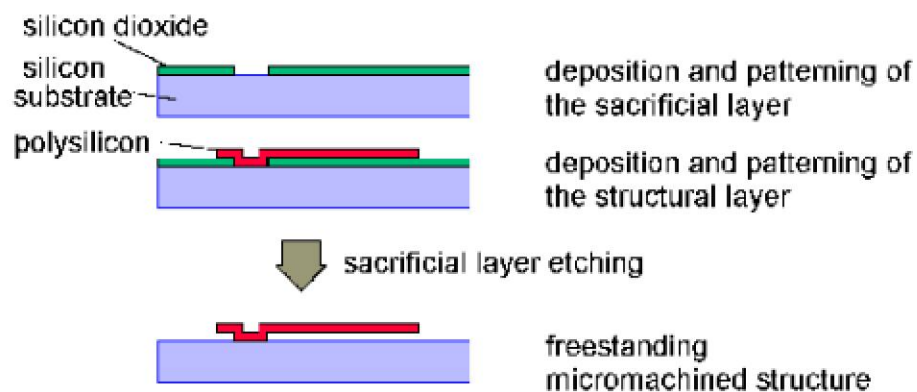
Figure 1-3 *Surface micromachining process*

6

1.2.3 LIGA process

LIGA is a fabrication process that produces high aspect ratio microstructures in X-ray lithography, electroforming, and plastic molding. This process overcomes some drawbacks of silicon-based micromachining technology. The LIGA process uses deep X-ray lithography to make desired patterns on a thick film of photoresist. X-rays are used as the light source in photolithography and provide excellent results for creating 3D microstructures with high aspect ratio MEMS devices [13]. There are three types of LIGA depending on the radiation source and preform used:

• X-ray LIGA using high-energy of X-rays

• UV-LIGA using ultraviolet light produced by a UV-lamp, and

• Silicon-LIGA using (Deep Reactive Ion Etching) DRIE-etched silicon

The substrate materials in LIGA processing are called the base plate, and various materials such as austenite steels, ceramics, and polymers are used to produce non-silicon-based microstructures. These materials must function as an electrical conductor or insulator. LIGA processes allow the creation of electric, magnetic, piezoelectric, and insulating properties in sensors and actuators. The LIGA process is usually applied to high precision micromachining as in motors, gears, actuators, and connectors. However, the technique is not ideal due to its high production costs [14]. Figure 1-4 shows a specific example of the LIGA process [4]. A thick film of photoresist material is deposited on top of a substrate as shown in 1-4a. The optical photoresist material for the LIGA process is PMMA (polymethyl methacrylate) because it is sensitive to X-rays. First, to block X-ray transmission, masks (Si_3N_4) are used in the X-ray lithography. Next, the deep X-ray dissolves the photo-resist material in 1-4b. This is followed by electroplating

of the PMMA photoresist with the desired metal in 1-4c. Finally, after removing the

photo-resist, the desired tube product is produced as shown in 1-4d.
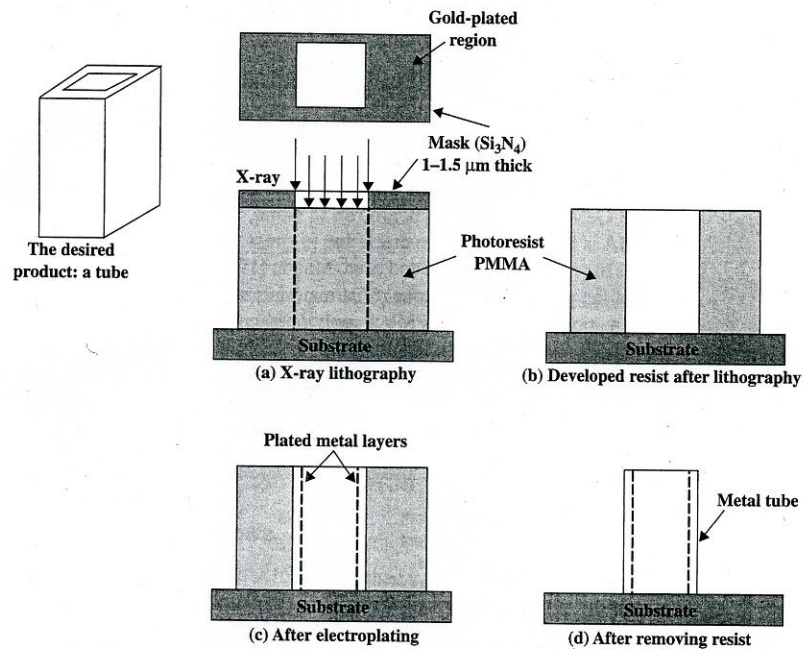
Figure 1-4 LIGA process

1.3 MEMS Applications

The first MEMS devices were applied to the automotive industry as airbag

accelerometers, which were integrated with electronics on a single chip [15]. These were

small, low-cost devices with a high degree of sensitivity. In addition, the high sensitivity

of MEMS devices was used to calculate passenger size and weight to help modulate the

airbag response. Digital micromirror devices (DMD) were invented by Texas Instruments

and had integrated large-scale, spatial light modulators [11, 16, 17]. The micromirror

devices made use of a transformable mirror array on microflexures, and are used in

airline-ticket laser printers and high-resolution projection devices. With increasing

demands for the MEMS market, the application has expanded into telecommunication, radio-frequency (RF) communication, biomedical and medical care applications [18].

1.3.1 Telecommunications

MEMS-based optical switches have become important since the late 1990s. Most of the components in optical MEMS telecommunication are operated by moving a reflective surface [19]. When the signal travels down the cables, it is converted from optical to electrical and back to optical in order to transfer from one line to another. Even though early attempts to integrate MEMS into this O-E-O conversion did not work, nut it become clear that electronic switching played a significant role in the network. Therefore, future cross-connects will be combined with hybrid optical and electrical devices.

1.3.2 RF MEMS

Radio Frequency (RF) MEMS is usually defined as the design and fabrication of MEMS for RF integrated circuits. The dramatic evolution of personal communication devices is attributable to the sophisticated RF MEMS. MEMS devices are applied to actuation or adjustment of a separate RF device or components, such as capacitors, switches, and filters [20]. In contrast to traditional RF devices, RF MEMS circuit design permitted development of components that are operated worldwide and has superior RF performance and tunability over a broader range of operating frequencies.

MEMS technology has been applied to other RF applications. Silicon-based RF MEMS technology was first used as microwave switches for surface micromachining actuators that provided low insertion loss, high linerarity, and low DC standby power

compared to traditional technology [21]. Table 1-1 shows the properties of RF MEMS according to switch types [22]. RF MEMS are also used as MEMS inductors and tunable capacitors for integrated voltage-controlled oscillators (VCOs) in global positioning systems (GPSs) [23]. Currently, the advantages of RF MEMS properties such as low power consumption and reconfigurability are making a worldwide wireless network more feasible.

Table 1-1 Properties of RF MEMS

Switch Type	Properties[1]					
	Insertion Loss	Isolation	Power Consumption	DC Voltage	Speed	Bandwidth
PIN/SCHOTTKY	~.15 dB	45 dB	1-5 mW per device	1-10 V	1-5 ns	Narrow/ Wide
GaAs FETs	1-2 dB	~20 dB	1-5 mW per device	1-10 V	2-10 ns	Narrow/ Wide
HBT/PIN	0.82 dB	25 dB	1-5 mW per device	1-10 V	1-5 ns	Narrow/ Wide
Best FET	0.5 dB	70 dB	5 mW	3.5 V	2 ns	Narrow/ Wide
MEMS – Sergio Shunt	0.06 dB @ 20 GHz	30 dB	~1μW	12-14 V	>30 μs	Wide (1-40 GHz)
MEMS – Scott/Jeremy(Shunt)	0.3 dB @ 30 GHz	50-60 dB	~1μW	~20 V	>30 μs	Moderate (10-40 GHz)

1.3.3 Biomedical and medical care applications

Recent progress in MEMS technology is being applied to biomedical and clinical medicine and has resulted in the creation of a new field of research known as bioMEMS. Currently, bioMEMS are used in microfluidics, cellular interactions, and biomolecular analysis. BioMEMS provide ever-greater functionalities and cost reductions for medical diagnostics and therapies. It also provides fast results from a single-array structure or

multi-array structure. Because of these advantages, MEMS are an important apparatus in the future of biomedical engineering and medical diagnostics. For example, drug delivery systems integrated with chemical sensors offer chemically-driven automated dose response [18, 24]. Recently, an isotachophoresis capillary electrophoresis system was developed for the protein diagnosis [25]. Figure 1-5 illustrates the application of bioMEMS.
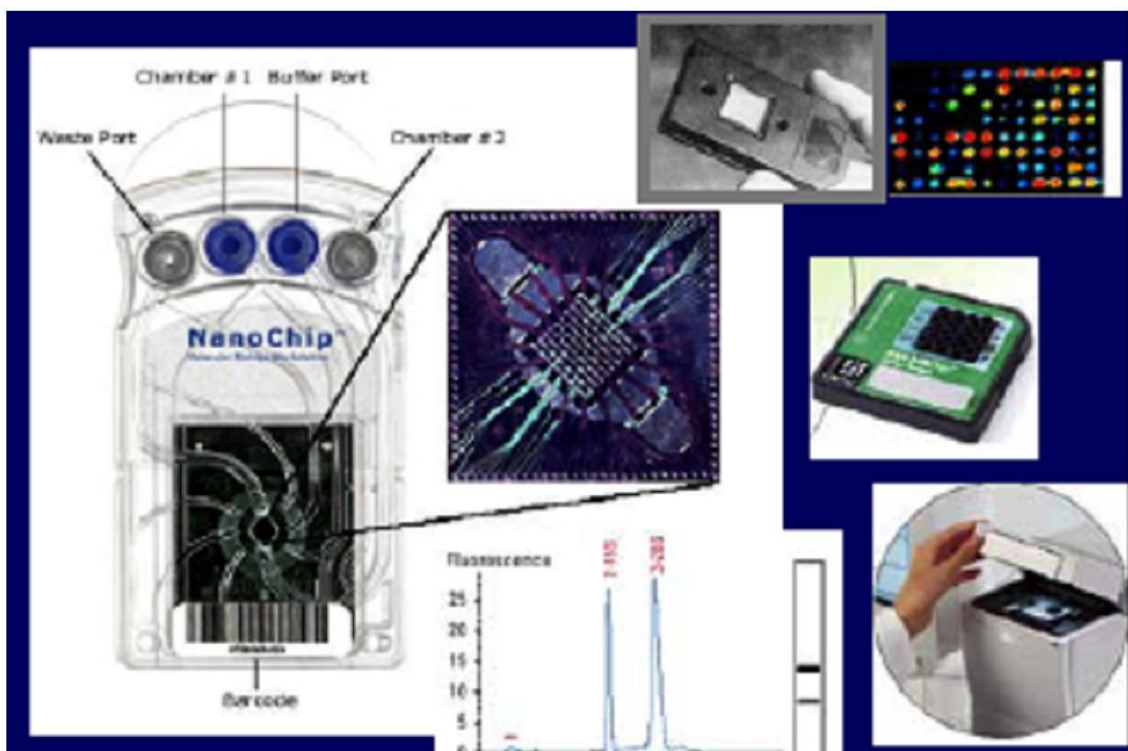
Figure 1-5 BioMEMS applications

1.4 Characteristics and Advantages of MEMS

Micro-Electro-Mechanical Systems (MEMS) are used in a range of applications. The advantages of MEMS go beyond the obvious benefit of their small size. The following section describes the advantages of MEMS.

1.4.1 Low cost

Over the past 50 years, the MEMS technology has produced highly functional, complex MEMS devices at low cost and in less time. Most of MEMS devices are batch fabricated so thousands or even millions of devices can be fabricated simultaneously.

1.4.2 Small size device

The small size of MEMS devices has the most powerful interest since microscopic devices are not feasible. With development of MEMS technology, building of complex mechanical elements with micrometer scale is possible. High performance of small size MEMS sensors can detect incredibly small signals.

1.4.3 Reliability

Most conventional mechanical devices fail at points of contact between components. MEMS technology provides better reliability by reducing the number of solder joints and wires [18]. MEMS devices are usually fabricated with a single monolithic structure that does not contain connectors, fasteners, and joints. To increase reliability, MEMS devices are typically sealed in a controlled environment to prevent corrosion and accumulation of dust. This also eliminates the need for lubricants, coolants, or maintenance.

1.4.4 Power consumption

Small sizes of MEMS devices typically consume less power. One good example of this is the electrostatic MEMS switch that only consumes nanowatts of power.

1.4.5. Performance

Operating on a micro-scale provides many advantages in performance and functionality. The low mass of MEMS devices allows them to act faster than conventional mechanical devices, leading to faster switches or higher bandwidth sensors.

1.5 References

[1] P. Sydenham, R. Thorn, *Handbook of Measuring System Design*, 1st Edn, John Wiley& Son Ltd, Chichester, UK (2005)

[2] A. A. G Requicha, C. Baur, A. Bugacov, B. C. Gazen, B. Koel, A. Madhukar, T. R. Ramachandran, R. Resch, P. Will, "Nanorobotic assembly of two- dimensional structures", *Proc. IEEE Int'l Conf. on Robotics & Automation*, 4, 3368-3374 (1998)

[3] R. Maboudian, C. Carraro, "Surface engineering for reliable operation of MEMS devices", *J. Adhesion Sci. Technol.*, 17, 583-591 (2003)

[4] T. Hsu, *MEMS & Microsystems Design and Manufacture*, 1st Edn, McGraw-Hill, New Jersey, United State (2002)

[5] Y. X. Zhuang, A. Menon, "On the stiction of MEMS materials", *Tribology letters*, 19, 111-117 (2005)

[6] M. Chandross, C. D. Lorenz, G. S. Grest, M. J. Stevens, E. B. Webb III, "Nanotribology of Anti-Friction Coating in MEMS", *JOM*, 57, 55-61 (2005)

[7] S. S. Perry, W. T. Tysoe, "Frontiers of fundamental tribological research", *Tribology letters*, 19, 151-161 (2005)

[8] R. Maboudian, *Fundamentals of Microfabrication*, 1st Edn, CRC Press, Florida, United State (1997)

[9] R. C. Jaeger, *Introduction to Microelectronic Fabrication*, 2nd Edn, Prentice Hall, New Jersey, United State (1988)

[10] J. Linke, D. M. Yohannes, G. Jost, B. Martin, L. Bernd, Y. Jin, A. Georg, S. Varshni, A. Gisela, G. Gabi, R. Ralf, D. Reinhard, "SU-8 based deep x-ray lithography/LIGA, *Proceedings of SPIE*, 4979, 394-401 (2003)

[11] S. Sundararajan, *Micro/nanoscale Tribology and Mechanics of Components and Coatings for MEMS*, Dissertation, Ohio State University, Columbus, 2001

[12] B. Bhusan, *Handbook of Micro/Nano Tribology*, 2nd Edn, CRC Pressure, Florida, United State (1998)

[13] E. W. Becker, W. Ehrfeld, P. Hagmann, A. Maner, D. Munchmeyer, " Fabrication of microstructures with high aspect ratios and great structural heights by synchrotron radiation lithography, galvanoforming, and plastic moulding (LIGA Process)", *Microelectronic Eng.*, 4, 35-56 (1986)

[14] R. A. Lawes, "Manufacturing costs for microsystems/MEMS using high aspect ratio microfabrication techniques", *Microsystem Technology*, 13, 85-95 (2007)

[15] D. S. Eddy, D. R. Sparks, "Application of MEMS technology in automotive sensors and actuators", *Proceedings of IEEE*, 86, 1747-1755 (1998)

[16] L. J. Hornbeck, "Digital light processing(TM) update- status and future applications (invited)", *Proc. Soc. Photo-Opt. Eng.*, 3634, 158-170 (1999)

[17] L. J. Hornbeck, W. E. Nelson, "Bistable deformable mirror device", *OSA Technical Digest Series*, 8, 107-110 (988)

[18] A. D. Romig, M. T. Dugger, P. J. McWhorter, "Materials issues in microelectromechanical devices: science, engineering, manufacturability, and reliability", Acta Materialia, 51, 5837-5866 (2003)

[19] J. Ford, "Telecommunications with MEMS devices: an overview", *Lasers and Electro-Optics Society*, 2, 415-416 (2001)

[20] V. Varadan, K. A. Jose, V. K. Varadan, U. Zoelzer, *RF MEMS and Their Applications*, 1st Edn, John Wiley& Son Ltd, Chichester, UK (2002)

[21] L. E. Larson, "Microwave MEMS technology for next-generation wireless communication", *IEEE MTT-S international symposium Digest*, <u>3</u>, 142-147 (1999)

[22] B. Pillans, G. Rebeiz, J. B. Lee, "Advances in RF MEMS Technology", *Gallium Arsenide Integrated Circuit (GaAs IC) Symposium, 2003. 25th Annual Technical Digest*, San Diego, CA, United State, November 2003

[23] H. Wu, A. Hajimiri, "Silicon-based distributed voltage-controlled oscillators", *IEEE Journal of Solid-State Circuits*, <u>36</u>, 493-502,

[24] N. Wilke, A. Morrissey, S. Ye, J. O'Brien "Fabrication of microneedle arrays for drug delivery using wet etch technologies", European Micro and Nano systems 2004, Paris, France, October 20-21, 2004

[25] S. J. Paik, S. W. Byun, J. M. Lim, Y. H. Park, A. Lee, S. Chung, J. G. Jang, K. J Chun, D. I. Cho, "In-plane single-crystal-silicon microneedles for minimally invasive microfluid systems", *Sensors and Actuators A-Physical*, <u>114</u>, 276-284 (2004)

CHAPTER 2

MEMS PERFORMANCE AND RELIABILITY

2.1 Materials For Microelectromechanical Systems (MEMS)

MEMS components are fabricated with a variety of materials depending on the specific application. However, silicon materials, metals, metal alloys, ceramics and polymers are most often used for MEMS manufacturing and are known internationally as a family of MEMS materials.

2.1.1 Silicon-based MEMS

Most simulated and fabricated MEMS devices have been based on silicon because it has excellent electronic and mechanical properties and has been extensively characterized, used, and manipulated in the semiconductor industry [1, 2]. Silicon is a very popular material:

• It is mechanically stable and can be easily integrated on a silicon substrate.

• It has a good Young's modulus.

• It has a high melting point at $1400°C$, which contributes to dimensional stability at elevated temperatures.

• Its thermal expansion coefficient is about 8 times smaller than that of steel and 10 times smaller than that of aluminum.

• The silicon wafer is extremely flat and allows chemical coating for surface modification.

17

• It offers a flexibility in design and manufacture, so treatment and fabrication processes are well established.

Because of the reliability of MEMS devices, a variety of chemical modifications to the polysilicon have been explored. Several chemical modification methods in the vapor and liquid phase have been applied to the contacting surface in MEMS and have been tested with microinstruments. However, intensive research is still needed in this area [3-5].

2.1.2 Metal and metal alloys-based MEMS

The growth of the MEMS industry motivates the discovery of new materials. Thin- film metals have been used in IC (Integrated Circuit) chips for several years which are a miniaturized electronic circuit, while most of the thick- film metals are commonly used for structural materials. For example, nickel, copper, and gold have been electroplated to make thick-film structures, and three dimensionally printed stainless steel microstructures have been fabricated by spatial forming technology [6]. Also, due to the composition and thickness limitations of Si micromachining, stainless steel nano-powder was used to fabricate parts for MEMS [7]. There are advantages in using electroplated metal. Electroplated metal is highly conductive, has high current capacities, and can be processed at low temperature. In addition, it can be used for both thin and thick layers due to low-cost and fast deposition. The rapid development of MEMS devices using metal has extended to RF MEMS, optical switches, and micro-mirror devices [8]. For example, mirror microfabrication has a simple metal deposition processes such as the sputtering process, which is often used to deposit thin metallic films on substrate surfaces.

Various metal alloys have been used on a number of MEMS devices. CoNiMn thin films were used for magnetic actuation, and TiNi shape memory alloy films were sputtered on the substrate for self-assembled monolayer (SAM) sensing and actuating [9, 10]. Recently, thin-film alloys of platinum (Pt), rhodium (Rh) and ruthenium (Ru) with gold (Au) were deposited on silicon substrates for MEMS switches [10].

2.1.3 Polymer MEMS

Polymers are an exciting new material for MEMS devices and can be used as both structural and functional materials. Polymers are widely used as photoresist, stamps for hot embossing and imprinting, conductors, and protective coatings for MEMS devices. BioMEMS, microfluidic devices, and various sensors use polymers because of their low cost, biocompatibility, high elasticity, optical properties, and high corrosion resistance. Table 2-1 shows a list of the structural polymers.

Among a variety of polymer materials, PMMA (polymethylmethacrylate) and SU-8 are the commonly used for MEMS devices. For instance, the adhesion forces of SU-8 and PMMA are 3~4 times smaller than those of a native oxide silicon layer. This small adhesion force means there is a small tendency of stiction. PMMA is called a versatile polymeric material because it has been commonly used as a high-resolution positive resist for e-beam, X-ray, and deep UV imaging. Furthermore, it is also used as a bonding adhesive, a sacrificial layer, and a thin film coating. Recently, a combination of silica and PMMA was reported in microfabrication [11]. Although PMMA offers excellent pattern quality and contrast, the SU-8 microstructures offer higher sensitivity than PMMA [12]. SU-8 is a negative photo-resist and the portion that is exposed to light

becomes insoluble to the photo-resist developer; the unexposed portion of photo-resist is removed by the photo-resist developer. MEMS market has explored SU-8 over the last few years and it is used in the manufacture of high aspect ratio microstructures [13-15]. The high aspect ratio is contributes to forming electroplated metal parts, micromolds for injection molding, and molding for polydimethylsiloxane (PDMS) structures. SU-8 can be patterned by X-ray, UV, and e-beam and has high sensitivity, chemical resistance, compatibility with electroplating, and low cost of negative resist [16]. Because of these benefits, SU-8 is considered to be an ideal photoresist material for MEMS technology.

2.2 Tribology of MEMS

Even though MEMS are easily integrated into multifunctional systems, have low power consumption due to their small size, and a low cost of manufacture, most MEMS failures occur at spots where two parts make contact. This interaction depends on the tribology- friction, adhesion, stiction, and wear phenomena. The concept of tribology originated in the UK in 1966 and can be defined as the science and technology of interacting surfaces in relative motion [17, 18]. The lifetime of MEMS devices and production yield is limited by tribological issues and has become a serious concern [19-21]. Unwanted adhesion and friction impacts the performance of MEMS devices and those phenomena are caused by large surface-to-volume ratios that cause adhesion to the underlying substrate or to nearby microstructures- also known as stiction [22]. Stiction phenomena are caused by a weak restoring force and are divided into release stiction and in-use stiction. The adhesion and friction properties are also dependent upon the materials used, surface roughness, relative humidity, temperature, velocity, and rest time [23, 24].

MEMS devices all experience normal or slide contact, friction, and wear during use and these interactions affect the lifetime of microdevices. Therefore, understanding interdisciplinary subjects like physics, chemistry, and material science is essential for the design and manufacture of MEMS devices. Occasionally, tribological problems are solved using computer simulations, which can prevent catastrophic failure. Computer simulation with a large number of components requires optimized parallel programs and is important for the development and testing of MEMS devices [25]. Since the fundamental issues describing surface interactions are not understood, it is currently difficult to develop accurate simulation programs. Further development of such software programs is warranted.

2.2.1 Interfacial forces

There are a number of tribological forces that are generated by MEMS devices on contacting surfaces. Inertial forces are the dominant contact forces in macro-scale surfaces, while other forces are dominant contact forces in micro-scale surfaces. If the length of the machine decreases from 1mm to 1μm, the surface area decreases by a factor of one million. This means that the surface area to volume ratio increases when the length of the machine decreases. Thus, inertial forces become less dominant and attractive surface forces play a more significant role [26]. Capillary, molecular van der Waals forces, and electrostatic forces interfere with the normal operation of MEMS devices [27-29]. Figure 2-1 compares the attractive force as a function of the separation between two smooth silicon surfaces within a 1μm*1μm area.

The strongest interfacial force is generated by water between two surfaces in a humid environment. When water vapor condenses in small crevices and pores, water forms a thin film at surface contact zones. Among the interfacial forces, the capillary force forms a large Laplace pressure when there is a small radius of curvature of the air/liquid interface and is a negative force against the force of gravity. The Laplace pressure pulls two surfaces together [30]. When the substrate is dried by evaporation, adhesion problems can arise. The adhesion value is about 10-100mJ/m^2 and depends on the size of the surface wetting area [24]

Electrostatic forces arise from a difference in contact potential, tribocharging of rubbing surfaces, and ion and/or electron trapping in oxide layers [28]. The term tribocharging describes the phenomenon of charge transfer by contact or rubbing [31]. The fundamental equation of electrostatic force is Coulomb's law that can be used to calculate the force between two charged plates. Coulomb's equation is

$$F = k\frac{q_1 q_2}{r}$$

where F is the force between charge 1 and charge 2, k is a constant, r represents the distance between two charges, q_1 is the quantity of charge on object 1, and q_2 is the quantity of charge on object 2. The calculated charge is either positive or negative. If q_1 and q_2 have the same sign, the repulsive force is dominant. If not, the attractive force is dominant. An excellent example of the importance of electrostatic forces is the RF MEMS switch. In this case, a switching element, a metallic membrane, is actuated by electrostatic force and contacts an electrode anchored to the substrate.
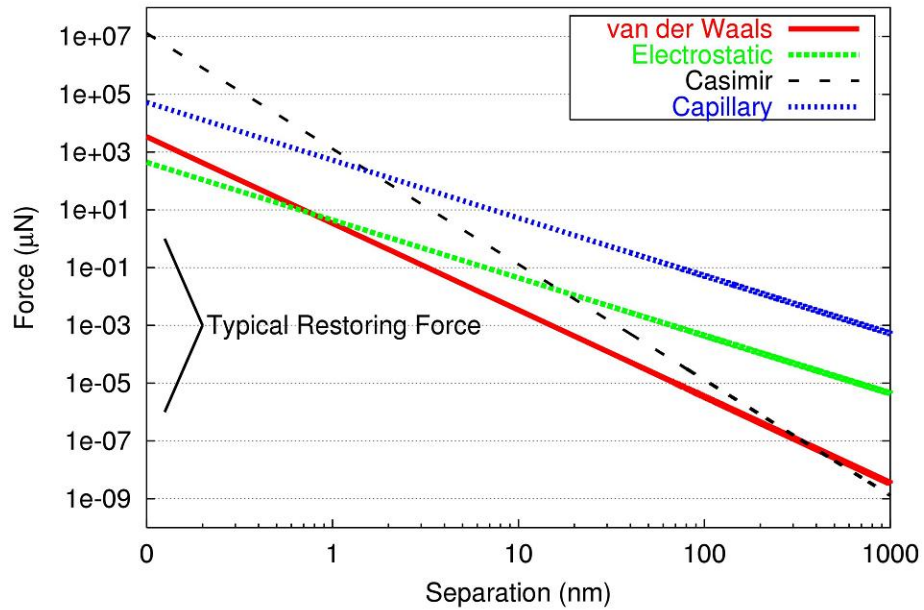
Figure 2-1 *Comparison of three attractive forces between perfectly flat silicon surfaces*

The molecular van der Waals forces are well known as attractive and long-range interfacial forces and refer to intermolecular forces in chemistry. Van der Waals is attraction/repulsion that is stronger than the dipole-dipole force, the dispersion force, and the hydrogen-bonding force. This force occurs when the surfaces are close enough, typically within a few nanometers, and it becomes more dominant than capillary force if the relative humidity is less than 30% or the surface roughness is less than 1nm [27].

2.2.2 Adhesion and stiction

With the development of MEMS technology, miniature device components can generate surface forces that are susceptible to forming undesirable adhesion between microstructures [32]. The term stiction refers to a combination of either one or more adhesion phenomena or adhesion forces at a contact area, and restoring forces that do not

encompass interfacial forces. The stiction phenomena usually occur during the release step of MEMS fabrication and are considered to be the most serious problems in MEMS devices [33]. Stiction occurs when two surfaces come in contact with each other under conditions where the adhesion force on the surfaces is larger than the other forces [27]. The strength of adhesion is controlled by surface forces such as capillary, electrostatic, and molecular van der Waals forces. In addition, surface roughness and chemical forces such as hydrogen bonding can generate adhesion. Figure 2-2 shows a typical stiction phenomenon between two surfaces. The stiction problems in MEMS technology are classified into two categories: release stiction and in-use stiction [34]. Release stiction occurs when the sacrificial layer is removed by microstructure fabrication processes and capillary forces are the dominant forces. In-use stiction occurs when microstructures are successfully released in a humid environment. If the surface attraction force is stronger than the restoring force, the surfaces become permanently fused and the device cannot operate [35].
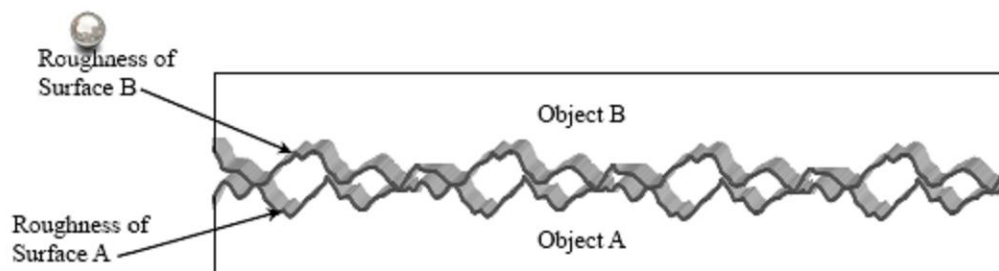

Figure 2-2 Schematic diagram of the stiction phenomenon between two surfaces

Stiction problems are complex and depend upon a variety of conditions. As seen in Fig 1.2, it is clear that the most important force among surface forces is capillary force, which occurs between liquid and solid interfaces. One possible way to reduce stiction is

24

to decrease the amount of water between the surfaces [27]. The capillary force between two plates can be expressed as shown in Figure 2-3:
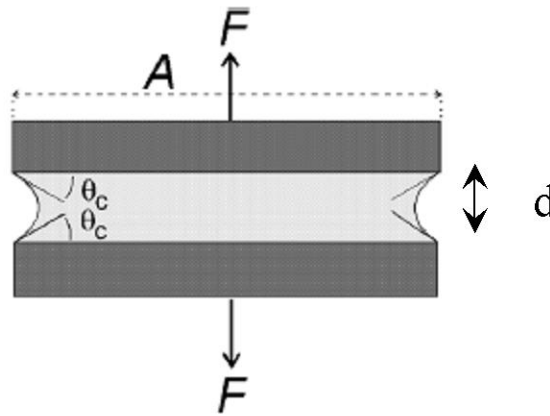
$$F = \frac{2A}{d} \gamma_{la} \cos\Theta_c$$

Where: γ_{la} = surface tension of the liquid-air interface

Θ_c = contact angle between liquid and solid

d = separation distance between two plates

A = area between two plates

Figure 2-3 *Capillary force between two plates*

Capillary forces depend on the relative humidity and temperature [36]. When the relative humidity increases and the temperature decreases, the stiction force increases. High relative humidity increases meniscus formation because more water is present in the environment. The water then condenses on the surface and this condensation causes stiction.

Surface roughness also plays a part in stiction. Due to non-uniformity of the oxide layer thickness, some parts are etched earlier than other parts, and the surface roughness

increases. The bumps or spaces on contacting surfaces can reduce the initial contact area, so the surface forces are effectively reduced [37]. There are possible ways to decrease stiction problems:

• use of stiff structures, so that the restoring forces can separate contacting layers

• use of rough surfaces to reduce contact surface area

• use of anti-stiction coatings such as self-assembled monolayers (SAMs)

• use of computer simulation to predict stiction in MEMS before manufacture [38,39]

2.2.3 MEMS friction and wear

Friction and wear of moving parts is a major concern for the reliability and performance of MEMS devices. A common MEMS material, silicon, has high friction and wear problems because unlubricated SiO_2 surfaces are very hydrophilic. Currently, the most complicated MEMS devices are rotary or linear-motion structures where sliding contacts occur. The most significant concerns in these devices are friction and wear [40]. At very low loads, the properties of friction and wear in macroscale are controlled by surface forces, while frictional force depends on the properties of the asperity at high loads. During the sliding, the interactions between asperities cause energy loss by means of elastic formation, plowing, and formation of wear debris [41].

2.2.3.1 Friction

Several experimental methods are used to measure frictional forces on smooth silicon and modified silicon surfaces. Atomic-Force Microscopy (AFM) is the most widely used instrument to measure frictional forces between tips and surfaces [42]. The

ultra-sharp tip of AFM is scanned across a surface [43]. However, these types of studies do not directly apply to surface-micromachining devices because of the unknown real contact area between the relatively rough polysilicon surfaces, and it is difficult to standardize surface phenomena due to variability in surface non-uniformity of LPCVD films [3].

Recently, Sandia National Laboratory has developed a new inchworm instrument, which moves in nanometer steps and can record friction information at the microscale. Using recently invented friction test devices, micromachined test structures have been used to characterize frictional forces in MEMS. Static friction forces were reported on oxidized polysilicon surfaces [3].

The first attempts to measure friction in MEMS originated from self-mated polysilicon in a vacuum and under various atmospheric conditions. The friction coefficients were around 0.2~0.8 and are related to sliding in a vacuum or inert atmospheres. Scale dependence of friction has been investigated by Nikhil and Bharat who found that the coefficient of friction was slightly increased with large scan sizes and large asperity sizes [30]. Another friction test as a function of pressure and velocity was investigated by using a cantilevered hinge-pad test structure [44].

Surface modifications such as self-assembled monolayers (SAMs) treatment have been developed to reduce friction problems, and several tests have been performed successfully. The coefficient of static friction in SiO_2 coating was 2.3± 0.8. Octadecyltrichlorosilane (OTS) and 1H, 1H, 2H, 2H-perfluorodecyltrichlorosilane (FDTS) can reduce the coefficient of static friction from 2.3± 0.8 to 0.13± 0.01 and 0.10± 0.007, respectively [30]. Friction tests with computer simulation have been conducted to

27

improve the reliability of MEMS devices. Based on theoretical studies, simulations can predict frictional properties, material properties, atmospheric conditions, and surface chemistry. One of the most important advantages over laboratory experiments is that computers can analyze friction at the atomic scale. Both the advances in computer hardware and development of software programs have enabled some successful computational studies [45, 46]

2.2.3.2 Wear

The operation of MEMS devices is highly dependent on the friction coefficient. However, wear will determine the longevity of MEMS devices and affects commercial and mechanical viability. Even though we know that silicon has good material properties such as high elastic modulus, low density, and small contact areas, it can suffer from plastic deformation due to high contact pressure. Wear is usually generated by the relative motions between two contacting surfaces. Figure 2-4 illustrates the wear phenomenon in a microengine pinhole before (a) and after (b) running. The proposed wear mechanisms in microengines are adhesive wear and abrasive wear [47]. The adhesive wear mechanism is applied to low contact pressure effects. Figure 2-5 shows the adhesive wear mechanism. Forces are applied to each surface and bring about contact at the asperity. When the lower surfaces begin to move, the asperities cold-weld together. If the lower surface moves continuously, the cold-weld breaks and the asperities increase. In contrast, abrasive wear is due to high contact pressure and a hard asperity grinding against contacting surfaces.
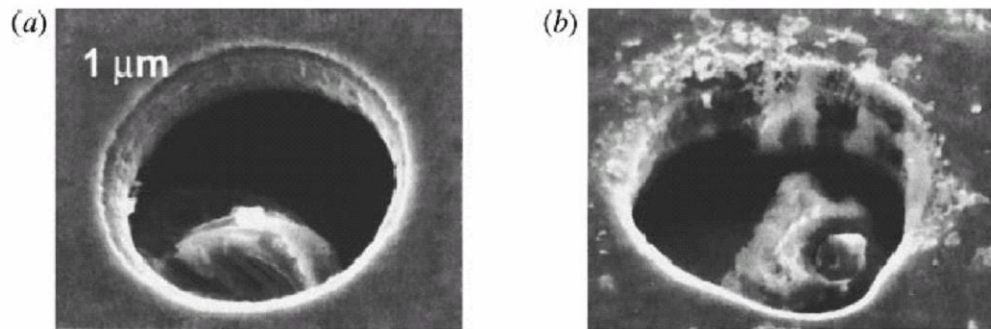
Figure 2-4 SEM images of a microengine pinhole before running (a), after running (b)

A variety of wear tests on silicon and its compounds have been examined. Single crystal silicon (SCS) microstructures coated with diamond-like carbon (DLC), silicon nitride (Si_3N_4), silicon dioxide (SiO_2), and doped and undoped polysilicon were examined to define the mechanical and chemical properties of those materials that contribute to the wear mechanism [48]. The results showed that DLC and SCS sliding on DLC decreased the wear rates when the sliding distance increased, while Si_3N_4 and SiO_2 showed approximately linear wear behavior. Tanner et al. reported on wear mechanisms and forces in driving load gear [49]. According to this research, the main failure was caused by wear at the sliding surface, and the coefficient of wear was dependent on wear volume, applied force, sliding length, and material strength. Tanner et al. also investigated the Sandia microengine in various conditions [50]. When MEMS devices are operated in very low humidity, large amounts of silver debris are found near the pin joint and hub. By contrast, under dry conditions, 40% relative humidity resulted in little silver debris. Li et al. examined nanowear properties of a MEMS test structure fabricated at Sandia National Laboratories using the atomic force microscope (AFM) and X-Ray Photoemission Spectroscopy (XPS) [51]. The results suggested that the morphology

29

present on the polysilicon surface will be worn flat during operation and will not adversely affect the wear properties of the polysilicon components.
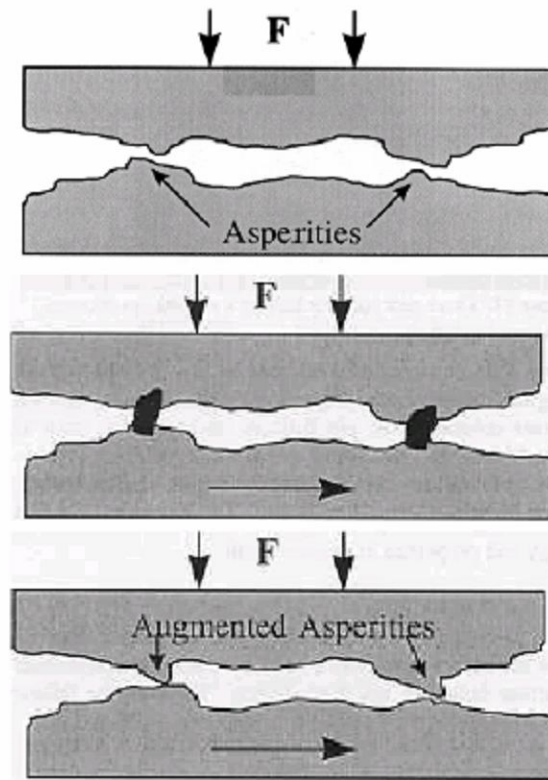

Figure 2-5 *Adhesive wear mechanisms*

Similar to experiments aimed at reducing friction problems, surface modification has been conducted to minimize wear. The selective deposition of tungsten on silicon is recognized as a successful wear-resistant coating [52]. The thickness of tungsten film is less than 20 nm, and the tungsten film helps increase the reliability of microengines. Thin SiC coatings also have excellent tribological properties and corrosion resistance [53]. Self- assembled monolayer coatings such as alkylsilane were used as lubricants on smooth silicon surfaces [54]. For example, alkylsilane-coated silicon structures seem to have a longer life when the chain length of the alkyl substituent is increased.

Recently, atomic layer deposition (ALD) has been applied to Si surface-micromachined structures. In spite of a variety of wear resistant coatings, several geometric constraints (high aspect ratio) still existed, but the ALD coating ensured a highly successful conformal and tribological coating on the surface. Because of these benefits, ALD is considered to be one of the most promising wear-resistant coatings. Al_2O_3 and TiO_2 are often used as precursors that adsorb until they saturate the surface and further growth cannot occur until the second precursor is introduced [55, 56]. For instance, 10nm thick films of Al_2O_3 used trimethyl group and water as precursors, while TiO_2 conformal coating used a single precursor, 1, 3- disilabutane (DSB).

2.3 MEMS coating

Since adhesion, friction, and wear were recognized as major concerns in the performance and reliability of MEMS devices, surface modification or coating have been widely used in MEMS devices to reduce tribological issues. Bowden and Tabor used a molecular coating to prevent stiction of a smooth indium ball [28]. This attempt was successful in preventing capillary condensation.

2.3.1 SAM coatings

Self-assembled monolayers (SAMs) are organic layers that have different structures and chain lengths. SAMs are used as a barrier layer that forms a uniform coating on the surface of microstructures and facilitates the release of microstructures. However, SAMs do not completely remove release stiction, but they do significantly alleviate in-use stiction [57].

Self-assembled monolayer coatings are deposited from a solvent. The organic solvent that promotes molecule dispersions reacts with waters on silicon surfaces for coating. An alkyltrichlorosilane with OH-terminated silicon is reacted with an amount of water. Covalent bonding of Si-O-R, and the cross-linking to other Si-O-R, produces a hydrophobic film on the silicon surface.

Alkyl- and perfluoroalkyl-trichlorosilane SAMs, dichlorosilane monolayer films, and alkene-based molecular films are specific examples of self-assembly monolayer coatings. Among these thin films, the most widely used silanes are octadecyltrichlorosilane (OTS), $CH_3(CH_2)_{17}SiCl_3$, and 1H, 1H, 2H, 2H-perfluorodecyltrichlorosilane (FDTS), $CF_3(CF_2)_7(CH_2)_2SiCl_3$. Figure 2-6 shows the processes of chlorosilane deposition onto a silicon surface. Tribological effects with SAM coatings were examined. The adhesion energy without surface modification is $56\mu J/m^2$, while MEMS surface energy after SAM treatment is $30\mu J/m^2$ for OTS, and $8\mu J/m^2$ for FDTS. Table 2-1 summarizes the physical properties of several SAM coatings [58]. In the case of two-step monolayer processes, the reactions arise from amine or alcohol functional groups on a chlorinated Si surface. This process yields a very effective assembly of organic layers that have a low surface energy and are thermally and mechanically stable [59].

When applied properly, self-assembled monolayers have the following characteristics on microstructure [60].

• They effectively remove release stiction.

• They alleviate in-use stiction. Compared to conventional oxidized release processes, SAMs is an effective method.

- They reduce friction in microengines.

- They exhibit strong persistence in harsh environmental conditions.

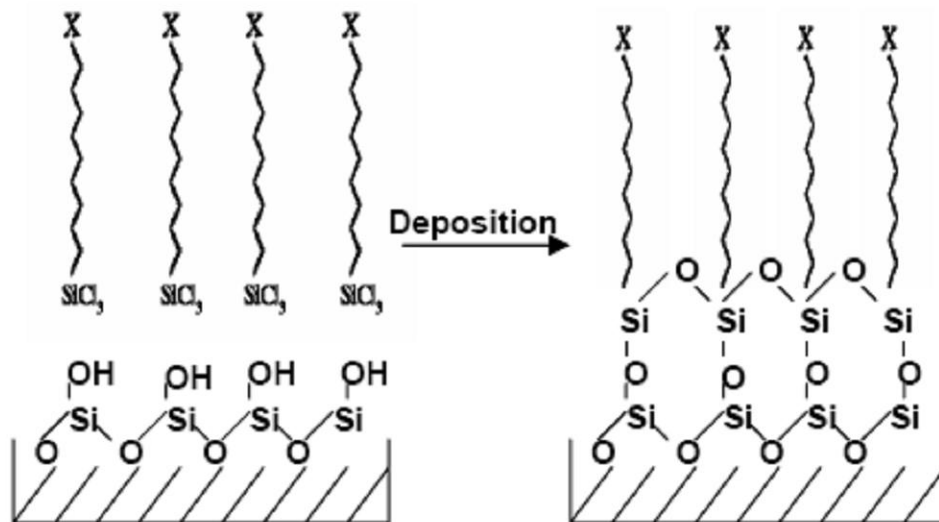- They do not require large input signals when microengines are starting up.

Figure 2-6 *Process of SAMs coatings*

Table 2-1 Summary of various SAMs coating properties

Surface Treatment	Water contact angle (°)	Work of adhesion (mJ/m^2)	Static friction coefficient	Thermal stability in air (°C)	Particulate formation
OTS	110	0.012	0.07	225	High
FDTS	115	0.005	0.10	400	Very high
DDMS	103	0.045	0.28	400	Low
1-octadecene	104	0.009	0.05	200	Negligible
Oxide	0–30	20	1.1	—	—

2.3.2 Vapor phase coating

Self-assembly monolayer coatings were usually deposited on the substrate by means of liquid deposition. However, vapor phase coating enables deposition of a hydrophobic layer by using vaporized precursor molecules. A recent development of coating technology, vapor phase coating is a useful tool:

• It eliminates the use of organic solvent and reduces chemical waste.

• It allows easy sample handling and implementation.

• Both full-wafer level and multi-wafer coatings are possible.

Even though vapor phase coating has attractive benefits, the results were not as good as for liquid-phase SAM coating [61]. The measured contact angle was between $70\sim100°$ and uniform coverage of surface was not achieved. With respect to successful separate release processes, supercritical CO_2 drying is a useful method [62].

2.3.3 Atomic Layer Deposition (ALD)

Since Atomic Layer Deposition (ALD) was first introduced as a new deposition technology, ALD methods and applications have developed rapidly over the last few years. ALD coating is a self-limiting and sequential surface chemistry. It forms highly uniform and conformal thin films of material onto substrates with varying compositions. ALD is similar to chemical vapor deposition (CVD). However, ALD breaks the CVD reaction into two half-reactions and separates the precursor materials. In chemical vapor deposition it is difficult to establish process control because of the sensitivity of reaction material flow, adsorption temperature, and time, while atomic layer deposition makes use of self-limiting mechanisms. ALD properties are different from CVD:

• Control of atomic scale deposition is achieved by means of self-limiting surface reactions.

• Conformal coating of high aspect ratio structures occurs with monolayer precision.

• Pin-hole free and chemically bonded to the substrate

• Various materials can be deposited (e.g. ceramics)

ALD film thickness depends on the number of deposition cycles. Figure 2-7 shows the processes using zirconium dioxide. First, $ZrCl_4$ vapor pulses in the chamber and forms an adsorption monolayer on the wafer surface. Second, water vapor is introduced into the chamber and reacts with the $ZrCl_4$ surface monolayer. This reaction forms a ZrO_2 monolayer. To increase the thickness, additional cycles could be performed. Conformal atomic layer coatings of TiO_2 [63], Al_2O_3 [55, 64], T_2O_5 [62] and ZrO_2 [63, 65] have been used to alleviate wear and friction [55, 63, 65]. These results suggest that ALD is one of the promising coating technologies in MEMS. Without a chlorosilane-based monolayer, alternative hydrophobic coating was introduced because of environmental safety concerns [64]. Herrmann et al. suggested that the adhesion energy of ALD coated cantilever was 0.11 ± 0.03 mJ/m at 100% humidity, while that of non-coated cantilever was 12 ± 1 mJ/m. The results show that non-chlorinated alkylsilanes are chemically bonded to hydroxyl groups on the ALD seed layer.
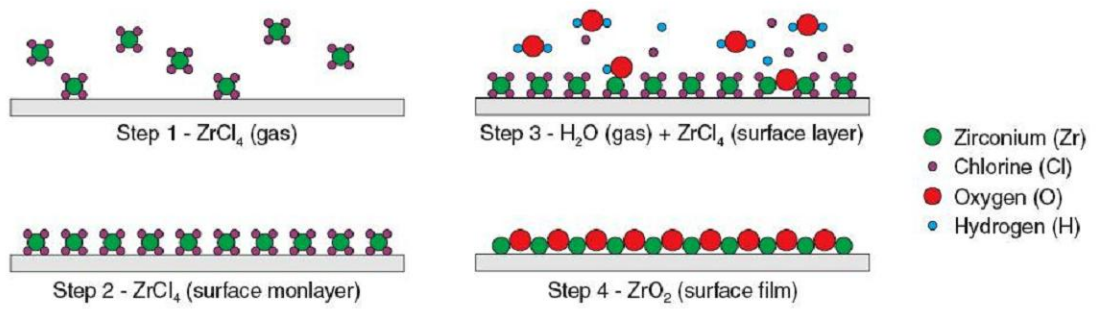
Step 1 - ZrCl$_4$ (gas)

Step 3 - H$_2$O (gas) + ZrCl$_4$ (surface layer)

Step 2 - ZrCl$_4$ (surface monlayer)

Step 4 - ZrO$_2$ (surface film)

● Zirconium (Zr)
● Chlorine (Cl)
● Oxygen (O)
● Hydrogen (H)

Figure 2-7 *Atomic layer deposition of zirconium dioxide*

2.4 References

[1] T. A. Core, W. K. Tsang, S. J. Sherman, "Fabrication technology for an integrated surface-micromachined sensor", *Solid State Technology*, <u>36</u>, 39-47 (1993)

[2] K. J. Gabriel, "Engineering Microscopic Machines", *Scientific American*, <u>273</u>, 118 (1995)

[3] R. Maboudian, C. Carraro, "Surface Chemistry and Tribology of MEMS", *Annu. Rev. Phys. Chem.*, <u>55</u>, 35-54 (2004)

[4] A. Ulman, *An Introduction to Ultrathin Organic Films: From Langmuir- Blodgett to Self-Assembly*, 1st Edn, Academic Press, New York, United State (1991)

[5] C. Carraro, L. Magagnin, R. Maboudian, "Selective Metallization of Silicon Micromechanical Devices", *Electrochim. Acta*, <u>47</u>, 2583-2588 (2002)

[6] C. S. Taylor, P. Cherkas, H. Hampton, J. J. Frantzen, B. O. Shah, W. B. Tiffany, L. Nanis, P. Booker, A. Salahieh, R. Hansen, "Spatial forming- A three dimensional printing process", Proceedings of IEEE MEMS 1995, Amsterdam, Netherlands, January 29- February 1, 1995

[7] T. J. Garino, A. Morales, T. Buchheit, B. Boyce, "The Fabrication of Stainless Steel Parts for MEMS", *Mat. Res. Soc. Symp. Proc.*, <u>687</u>, B5.19.1-B5.19.6 (2002)

[8] T. Becker, T. Bifano, H. Lee, M. Miller, P. Bierden, S. Cornelissen, "MEMS spatial light modulators with integrated electronics", Proceeding of SPIE, <u>4983</u>, 248-258 (2003)

[9] C. H. Ahn, M. G. Allen, "Micromachined planar inductors on silicon wafers for MEMS applications", *IEEE Transactions on Industrial Electronics*, <u>45</u>, 866-876 (1998)

[10] A. Ohta, S. Bhansali, I. Kishimoto, A.Umeda, "Development of TiNi shape memory alloy film deposited by sputtering from separate Ti and Ni targets", *Proceeding of SPIE*, 3512, 138-145 (1998)

[11] S. Juodkazis, K. Yamasaki, A. Marcinkevicius, V. Mizeikis, "Microstructuring of silica and polymethylmethacrylate Glasses by Femtosecond Irradiation for MEMS Applications", *Mat. Res. Soc. Symp. Proc.*, 687, B5.25.1-B5.25.5 (2002)

[12] L. Jian, Y. M. Desta, J. Goettert, M. Bednarzik, B. Loechel, J. Y. Young, G. Aigeldinger, V. Singh, G. Ahrens, G. Gruetzner, R. Ruhmann, R. Degen, " SU-8 based deep X-ray lithography/LIGA", *Proceedings of SPIE*, 4979, 394-401 (2003)

[13] N. C. LaBianca, J. D. Gelorme "High aspect ratio resist for thick film applications", *Proceedings of SPIE*, 2438, 846-852 (1995)

[14] A. L. Bogdanov, S. S. Peredkov "Use of SU-8 photoresist for very high aspect ratio X-ray lithography", *Microelectronic Engineering*, 53, 493-496 (2000)

[15] E. H. Conradie, D. F. Moore, "SU-8 thick photoresis processing as a functional material for MEMS applications", *J. Micromech. Microeng.*, 12, 368-374 (2002)

[16] H. Lorenz, M. Despomt, N. Fahrni, N. LaBianca, P. Renaud, P. Vettiger, "SU-8: a low-cost negative resist for MEMS", *J. Micromech. Microeng.*, 7, 121-124 (1997)

[17] S. S. Perry, W. T. Tysoe, "Frontiers of fundamental tribological research", *Tribology letter*, 19, 151-161 (2005)

[18] B. Bhushan, *Principles and applications of tribology*, John Wiley& Sons, Inc.; 1999

[19] R. Maboudian, "Adhesion and friction issues associated with reliable operation of MEMS", *Materials Research Society Bulletin*, 23, 47-51 (1998)

[20] R. Maboudian, R. T. Howe "Critical review: adhesion in surface micromachined structure", *J. Vac. Sci. Technol. B*, 15, 1-20 (1997)

[21] K. Komvopoulos, "Surface engineering and microtribology for microelectromechanical systems", *Wear*, 200, 305-327 (1996)

[22] M. P. de Boer, T. M. Mayer, "Tribology of MEMS", *MRS Bulletin*, 302-304 (2001)

[23] H. Liu, B. Bhushan, "Adhesion and friction studies of microelectromechanical systems/nanoelectromechanical systems materials using a novel microtriapparatus", *J. Vac. Sci. Technol. A*, 21, 1528-1538 (2003)

[24] M. P. De Boer, P. J. Clews, B. K. Smith, T. A. Michalske, "Adhesion of polysilicon microbeams in controlled humidity ambient", *Mat. Res. Soc. Symp. Proc.*, 518, 131-136 (1998)

[25] T. Cagin, J. Che, M. N. Gardos, A. Fijany, W. A. Goddard III, "Simulation and experiemtns on friction and wear of diamond: a material for MEMS and NEMS application", *Nanotechnology*, 10, 278-284 (1999)

[26] R. Maboudian, C. Carraro, "Surface Chemistry and Tribology of MEMS", *Annual Review of Physical Chemistry*, 55, 35-54 (2004)

[27] W. M. V. Spengen, R. Puers, I. D. Wolf, "On the physics of stiction and its impact on reliability of microstructures", *J. Adhesion Sci. Technol.*, 17, 563-582 (2003)

[28] J. A. Williams, H. R. Le, "Topical Review Tribology and MEMS", *J. Phys. D: Appl. Phys.*, 39, R201-R214 (2006)

[29] J. Li, Z. Cui, M. A. Baker, "A study of the surface chemistry, morphology and wear of silicon based MEMS", *Surface and Interface Analysis*, 36, 1254-1258 (2004)

[30] N. S. Tambe, B. Bhushan, "Scale dependence of micro/nano-friction and adhesion of MEMS/NEMS materials, coatings and lubricants", *Nanotechnology*, 15, 1561-1570 (2004)

[31] M. P. Damodar, B. E. Springett, "Physics of electrophotography", *Rev. Mod. Phys.* 65, 163 - 211 (1993)

[32] J. W. Rogers, L. M. Phinney, "Nanosecond Laser Repair of Adhered MEMS Structures", *Journal of Heat Transfer*, 124, 394-396 (2002)

[33] O. Raccurt, F. Tardif, F. A. d'Avitaya, T. Vareine, "Influence of liquid surface tension on stiction of SOI MEMS", *J. Micromech. Microeng.*, 14, 1083-1090 (2004)

[34] Y. P. Zhao, L. S. Wang, T. X. Xu, "Mechanics of adhesion in MEMS- a review", *J. Adhesion Sci. Technol.*, 17, 519-546 (2003)

[35] J. A. Williams, H. R. Le, "Some aspects of tribological behaviour at the micro-scale – with particular reference to MEMS and MMAS", Proceedings of Lyon-Leeds Tribology Conference 2004, Leeds, United Kingdom, September 7-10, 2004

[36] W. M. Spengen, R. Puers, I. D. Wolf, "On the physics of stiction and its impact on the reliability of microstructures", *Journal of Adhesion Science and Technology*, 17, 563-582 (2004)

[37] N. Tas, T. Sonnenberg, H. Jansen, R. Legtenberg, M. Elwenspoke, "Stiction in surface micromachining", *J. Micromech. Microeng.*, 6, 385-397 (1997)

[38] W. M. V. Spengen, R. Puers, I. D. Wolf, "A physical model to predict stiction in MEMS", *J. Micromech. Microeng.*, 12, 702-713 (2002)

[39] A. Y. Suh, A. A. Polycarpou, "Adhesion and Pull-off Forces for Polysilicon MEMS Surfaces Using the Sub-Boundary Lubrication Model", *Journal of Tribology*, 125, 193-199 (2003)

[40] J. J. Sniegowski, M. P. De Boer, "IC-Compatible Polysilicon Surface Micromaching", A*nnual Review of Materials Science*, 30, 299-333 (2000)

[41] D. W. Brenner, "Mysteries of Friction and Wear Unfolding: CMS Advances the Field of Tribology", *Advanced Materials and Processes Technology*, 5, 3-6 (2001)

[42] S. Sundararajan, B.Bhushan, "Static friction and surface roughness studies of micromachined electrostatic micromotors using an atomic force/friction force microscope", *J. Vac. Sci. Technol. A*, 19, 1777-1785 (2001)

[43] B. Bhushan, J. Israelachvili, U. Landman, "Nanotribology: Friction, Wear and Lubrication at the Atomic Scale", *Nature*, 374, 607-616 (1995)

[44] M. P. de Boer, J. M. Redmond, D. F. Bahr, T. A. Michalske, "Hinged-pad test structure for sliding friction measurement in micromachining", *Proceedings of SPIE materials and device characterization in micromaching*, 3512, 241-250 (1998)

[45] J. Shimizu, H. Eda, M. Yoritsune, E. Ohmura, "Molecular dynamics simulation of friction on the atomic scale, *Nanotechnolgy*, 9, 118-123 (1998)

[46] L. Zhang, H. Tanaka, "Towards a deeper understanding of wear and friction on the atomic scalema molecular dynamics analysis", *Wear*, 211, 44-53 (1997)

[47] D. M. Tanner, K. A. Peterson, L. W. Irwin, P. Tangyunyong, W. M. Miller, W. P. Eaton, N. F. Smith, M. S. Rodgers, "Linkage design effect on the reliability of surface micromachined microengines driving a load", *Proceedings of SPIE*, 3512, 215-226 (1998)

[48] U. Beerschwinger, D. Mathieson, R. L. Reuben, S. J. Yang, "A study of wear on MEMS contact morphologies", *J. Micromech. Microeng.*, 4, 95-105 (1994)

[49] D. M. Tanner, W. M. Miller, W. P. Eaton, L. W. Irwin, K. A. Peterson, M. T. Dugger, D. C. Senft, N. F. Smith, P. Tangyunyong, S. L. Miller, "The effect of frequency on the lifetime of a surface micromachined microengine driving a load", IEEE International Reliability Physics Symposium Proceedings 1998, Reno, Nevada, United State, March 30-April 2, 1998

[50] D. M. Tanner, J. A. Walraven, L. W. Irwin, M. T. Dugger, N. F. Smith, W. P. Eaton, W. M. Miller, S. L. Miller, "The effect of humidity on the reliability of a surface micromachined microengine", IEEE International Reliability Physics Symposium Proceedings 1999, San Diego, CA, United State, March 21 - 25 ,1999

[51] J. Li, Z. Cui, M. A. Baker, "A study of the surface chemistry, morphology and wear of silicon based MEMS", *Surf. Interface Anal.*, 36, 1254-1258 (2004)

[52] S. S. Mani , J. G. Fleming, J. J. Sniegowski , M. P. De Boer, L. W. Irwin , J. A. Walraven, D. M. Tanner, M. T. Dugger , "Chemical vapor deposition coating for micromachines", *Mater. Res. Soc. Symp. Proc.: Methods, Mechanisms and models of vapor deposition*, 616, 21-28 (2000)

[53] W. R. Ashurst, M. B. J. Wijesundara, C. Carraro, R. Maboudian, "Tribological impact of SiC encapsulation of released polycrystalline silicon microstructures", *Tribology Letter*, 17, 195-198 (2004)

[54] V. Kapila, P. A Deymier, S. Raghavan, "Molecular dynamic simulations of friction between alkylsilane monolayers", *Modeling Simul. Mater. Sci. Eng.*, 14, 283-297 (2006)

[55] T. M. Mayer, J. W. Elam, S. M. George, P. G. Kotula, R. S. Goeke, "Atomic-layer deposition of wear-resistant coatings for microelectromechanical devices", *Applied Physics Letters*, 82, 2883-2885 (2003)

[56] W. R. Ashurst, Y. J. Jang, L. Magagnin, C. Carraro, M. M. Sung , R. Maboudian, "Nanometer-Thin Titania Films with SAM-level Stiction and Superior Wear Resistance for Reliable MEMS Performance", Proceedings of IEEE MEMS Conference 2004, Maastricht, the Netherlands, January 2004

[57] R. Maboudian, C. Carraro, "Surface engineering for reliable operation of MEMS devices", *J. Adhesion Sci. Technol.*, 17, 583-591 (2003)

[58] X. Y. Zhu, J. E. Houston, "Molecular lubricants for silicon-based microelectromechanical systems (MEMS): a novel assembly strategy, *Tribology Letters*, 7, 87-90 (1999)

[59] R. Maboudian, W. R. Ashurst, C. Carraro, "Tribological challenges in micromechanical systems", *Tribology Letters*, 12, 95-100 (2002)

[60] S. H. Lee, M. J. Kwon, J. G. Park, Y. K. Kim, H. J. Shin, "Preparation and characterization of perfluoro-organic thin films on aluminium", *Surf. Coat. Technol.*, 112, 48-51 (1999)

[61] T. M. Mayer, M. P.de Boer, N. D. Shinn, P. J. Clews, T. A. Michalske, "Chemical vapor deposition of fluoroalkylsilane monolayer films for adhesion control in microelectromechanical systems", *J. Vac. Sci. Technol. B*, 18, 2433-2440 (2000)

[62] D. M. Hausmann, P. de Rouffignac, A. Smith, R. Gordon, D. Monsma, "Highly conformal atomic layer deposition of tantalum oxide using alkylamide precursors", *Thin Solid Films*, 443, 1-4 (2003)

[63] C. Nistorica, J. F. Liu, L. Gory, G. D. Skidmore, F. M. Mantiziba, B. E. Gnade, J. Y. Kim, "Tribological wear studies of coatings fabricated by atomic layer deposition and by successive ionic layer adsorption and reaction for microelectromechanical devices", *J. Vac. Sci. Technol. A*, <u>23</u>, 836-840 (2005)

[64] C. F. Herrmann, F. W. DelRio, V. M. Bright, S. M. George, "Conformal hydrophobic coatings prepared using atomic layer deposition seed layers and non-chlorinated hydrophobic precursors", *Journal of micromechanics and microengineering*, <u>15</u>, 984-992 (2005)

[65] J. F Liu, C. Nistorica, L. Gory, G. D. Skidmore, F. M. Mantiziba, B.E. Gnade, "Layer-by-layer depostion of zirconium oxide films from aqueous solutions for friction reduction in silicon-based microelectromechanical system devices", *Thin Solid Films*, <u>492</u>, 6-12 (2005)

CHAPTER 3

UNIFORM CONTROL OF THE DENSITY OF FUNCTIONALIZED GOLD NANOPARTICLES ON A MODIFIED SILICON SURFACE

3.1 Introduction

Nanoparticles have a variety of potential applications [1]. There is no accepted international definition, but nanoparticles are less than 100nm in size and maintain crystalline structures [2]. Among nanoparticles, gold nanoparticles have been widely used in the field of biosensors and bioMEMS because of their compatibility with biological systems [3-7]. Currently, gold nanoparticles can be applied to MEMS tribology because of their contributions to the analysis of friction and adhesion properties [8, 9].

However, gold nanoparticles have limitations because of their properties and morphology [10, 11]. Because of van der Waals attraction between particles they can be easily formed into clusters, which are made of several gold nanoparticles, unless immobilized [12, 21]. Furthermore, the scattering of gold nanoparticles becomes complicated during immobilization because of strong near-field interactions between the particle and the substrate [13]. Gold nanoparticles exist either as a colloid or as a solid. Aggregation in colloid gold nanoparticles can be easily detected by color changes [14]. Ligand stabilized gold nanoparticles that efficiently prevents aggregation are easily made

[15, 16]. Colloid gold nanoparticles are effective materials with respect to reducing steric hindrance and can create a well-organized silicon surface [3].

The control of the density of gold nanoparticles is an important area of study, and could help to maximize their use in a variety of industries. However, only a few such studies that concentration on important parameters of gold nanoparticle colloid solutions like the [3, 10, 17, 18], deposition time [3, 10, 19], reaction time [20] and pH of the solution [20, 21] exist. In addition, contamination of the silicon surface and surface roughness are important issues. Surface contamination gives rise to unexpected small size grains in the silicon surface that makes it difficult to distinguish between gold nanoparticles and polymeric particles. Therefore, effective wafer cleaning techniques are essential for the analysis of gold nanoparticle deposition on the surface during wet-chemical or gas/vapor phase dry processes [22, 23]. Surface roughness is important to obtain accurate information about the size distribution of nanoparticles because of the complex structure of the substrate surface on which the particles are placed [24].

Here, we demonstrated simple and effective ways to control the gold nanoparticle density on the silicon surface. Silicon has attractive properties including low cost, a flat and clean surface, and ease of microfabrication. Moreover, surface modification allows attachment of organic functional groups to the silicon surface [25-29]. The method of immobilization of the modified gold nanoparticles and silicon surface used in this study is depicted in Figure 3-1. The surface was modified by 3-MPTMS (Mercaptopropyltrimethoxylsilane), and thiolate-coated gold nanoparticles were used to reduce steric hindrance at the surface. Silanol-terminated silicon substrates allow very low coverage, so surface modifications as well as the gold nanoparticle ligands that are

changed by 3-MPTMS are the most significant factors [30]. The particle ligand maintains chemical stability. As a result, gold nanoparticles can be deposited on a chemically well-organized silicon surface, which also minimizes repulsive interparticle interactions. From AFM images and particle analysis tools, we learned that the density of gold nanoparticles depends on the concentration of colloid gold nanoparticles, deposition time, and 3-MPTMS concentration. Temperature did not seem to be a major factor. However, we found that some factors limit the ability to control gold nanoparticles density. Therefore, understanding of density control techniques on a silicon surface will allow us to develop more reliable gold nanoparticle-based electronic devices.
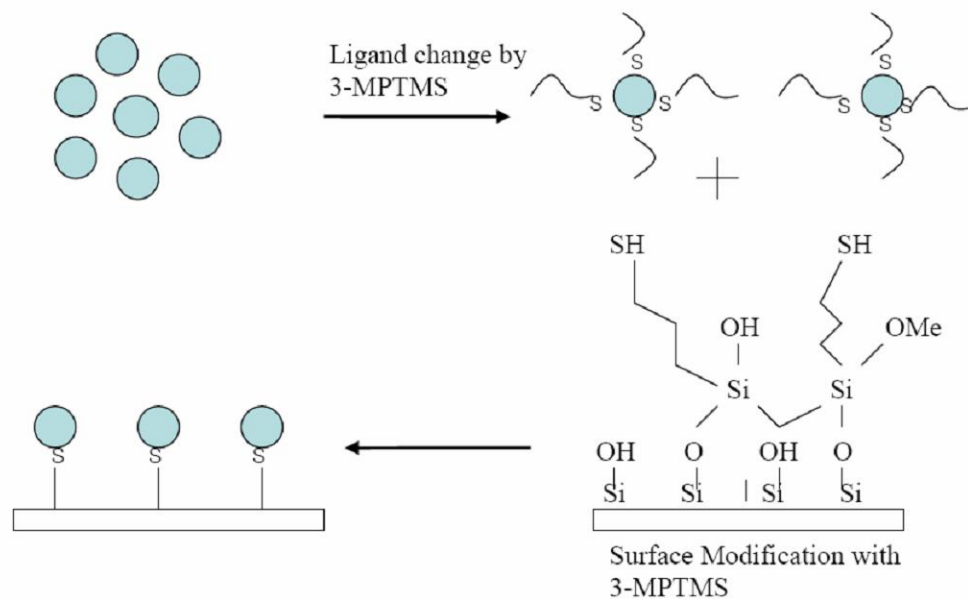
Figure 3-1 *Schematic representation for immobilization*

3.2 Experimental

3.2.1 Silicon wafer cleaning

Silicon wafers <100> (1cm×1cm) were cleaned by sonication in acetone for 10~15 minutes, and then dried with nitrogen gas. After the sonication process, the silicon wafer was dipped into HF solution (hydrofluoric acid, Fisher Scientific) for 10 minutes to remove polymeric particles. The HF-treated silicon wafer was completely washed with deionized waters until the pH reached 7, and was again dried with nitrogen gas. The silicon wafer was treated with oxygen and water plasmas for 5 minutes, each. After this, the measured contact angle was 0 degrees. The HF and plasma processes were repeated at least 3 times to completely remove polymeric particles.

3.2.2 Silicon and gold nanoparticle modification

The colloid gold nanoparticles (BBInternational, 40nm) were used for attaching material onto silicon surfaces. To maintain a uniform distribution, the silicon wafer was functionalized by 3-MPTMS (Mercaptopropyltrimethoxylsilane, Fisher Scientific). We assume that methoxy groups strongly react to the silicon surface, and sulfur in 3-MPTMS can react with gold nanoparticles. The gold nanoparticle solution consisted of 10 ml isopropanol (Fisher Scientific), gold nanoparticles (1~20 drops, 1 drop≈ 0.0124ml), and 3-MPTMS (1~7 drops). The solution was mixed by shaking more than 10 times and then the silicon sample was dipped into the gold nanoparticle solution.

3.2.3 Gold nanoparticle concentration effect

Concentration effects of the gold nanoparticle solution effect were investigated by increasing the number of drops of colloid gold nanoparticle solution. The final solution contained 10 ml isopropanol, 1 drop of 3-MPTMS, and either 1, 10, or 20 drops of BBInternational gold nanoparticles and was mixed for 1 hr.

3.2.4 Gold nanoparticle deposition time effect

Silicon samples were dipped into the gold nanoparticle solution prepared with 10ml isopropanol, 1 drop of 3-MPTMS, and either 1 or 20 drops of BBInternational gold nanoparticles for 1 to 3 hours.

3.2.5 3-MPTMS effect

The effect of 3-MPTMS concentration effect was investigated by increasing its concentrations. The gold nanoparticle solution was prepared with 10ml isopropanol, 1 drop of BBI gold nanoparticles, and different amounts of 3-MPTMS solutions (1, 3, 5, or 7 drops). The silicon samples were immersed into the solutions for 1 hour.

3.2.6 Temperature effect

The base solution consisted of 10ml isopropanol, 1 drop of 3-MPTMS, and 1 drop of BBInternational gold nanoparticles and was heated on a hot-plate (Fisher Scientific) to 43°C. The silicon samples were immersed in the solution for 1hr.

3.2.7 Analysis by Instruments

Microscopic imaging of the silicon surface and aqueous solutions of BBI gold nanoparticles were performed by AFM in the tapping mode (Pacific Nanotechnology, Nano-R^{TM}). The atomic force microscope is a very useful instrument but lacks the analytical ability to distinguish particles features. The shape of gold nanoparticles was confirmed by transmission electron microscopy (TEM) (Zeiss, EM 10C/10CR). The sample was prepared on a TEM grid (Ted Pella Inc.) from the colloid gold nanoparticle solution. Hydrophilic silicon surfaces roughness after treatment with oxygen plasma was examined by goniometer (Rame-hart Inc., Model 200) and chemical analysis of gold nanoparticles after ligand change was observed by SEM-EDS (Horiba, EMAX 3700).

3.3 Results and Discussions

After silicon sample cleaning, the silicon surface was scanned by AFM, and the scan size of the AFM image was 9.78 μm $\times$ 9.78 μm. Figure 3-2 shows a clean silicon surface image. Polymeric particle size by line analysis was 4.6 nm and surface roughness was 0.17 nm. The average sizes of particles from unwanted chemical reactions were 4~ 5 μm. A few polymeric nanoparticles were found as dim spots, while gold nanoparticles were detected by light spots in the AFM images.

Line Analysis

	Pair 1		Pair 2		Line 1	
	X (뮴)	Z (nm)	X (뮴)	Z (nm)	Total Length Rt.	9.78 뮴
Line1 1	3.758	5.495			Roughness Avg. Ra:	0.17 nm
2	3.592	0.903			Root mean square Rq:	0.42 nm
distance	-0.166	-4.592			Ten Points Height Rz:	1.20 nm
pt.angle	1.58 ?				Range Rr:	4.98 nm
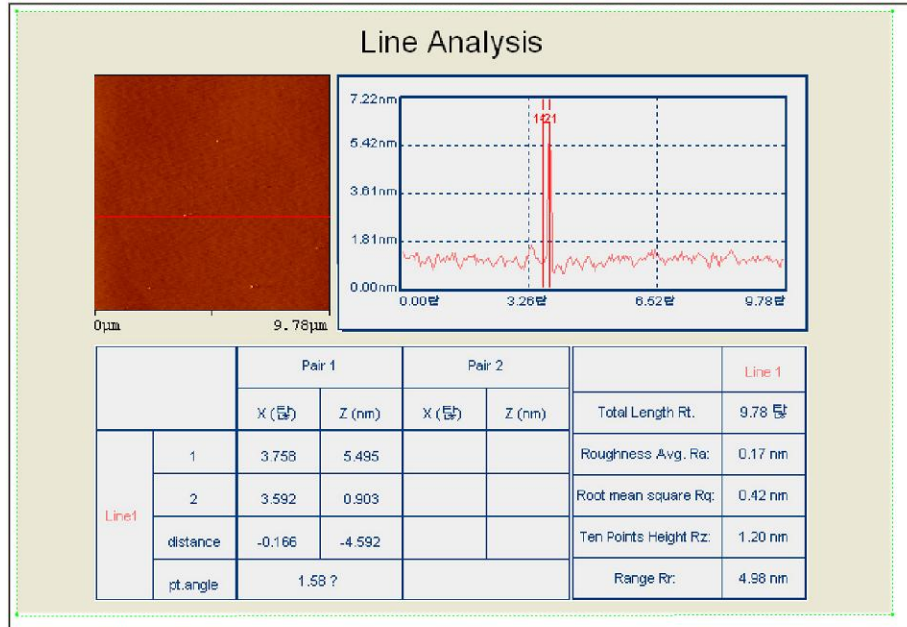
Figure 3-2 *AFM clean silicon image and line analysis*

The diameter of gold nanoparticles can be determined from either AFM or TEM. BBI gold nanoparticle (40nm) solution contains 9.0×10^{10} nanoparticles/ml. One drop of gold nanoaprticle solution is allowed to contact the silicon surface, and the resulting particle size distribution was analyzed by measuring the height of the particles in the AFM image. However, silicon surfaces were not treated to prevent aggregation, so some of gold nanopartice sizes were about 100 nm. Figure 3-3 shows AFM particle analysis software, and a height distribution of nanoparticles is shown in Figure 3-4. In Fig. 3-4, we ignored the aggregated gold nanoparticles in which particle sizes were above 40 nm. The mean size of the particles was about 26 nm. Because of the particle size differences, transmission electron microscopy (TEM, EM 10CR) was used for further microscopic characterization.

We found that the BBI 40nm gold nanoparticles were not completely spherical, as shown by the TEM image in Figure 3-5. Transmission electron microscopy (TEM) measures the transmitted electron beam after it passes through the sample and allows detection of an extreme lower size limit (below 0.2 μm) even though much of the three-dimensional information is lost. AFM is widely used to visualize 3-D structure and the tip is scanned on the substrate surface on which the particles are placed. Therefore, if the shape of the gold nanoparticles is not completely spherical, particle size analysis is not able to correctly process using AFM images [24].
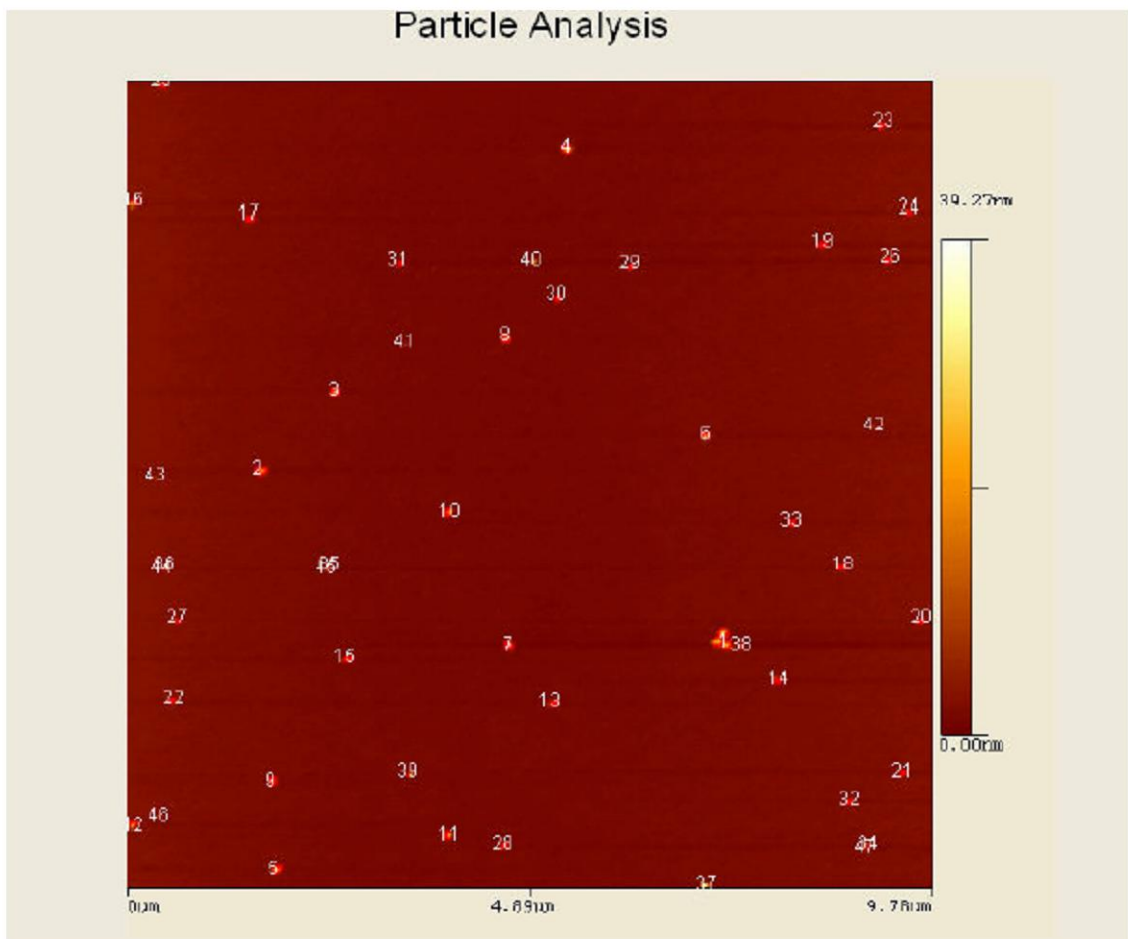
Figure 3-3 Particle analysis tool in AFM
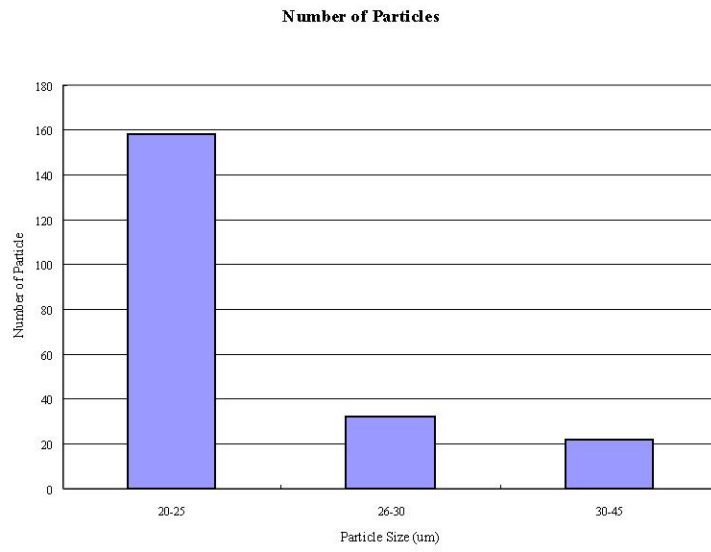
Range(nm)	Number of Particles
20-25	158
26-30	32
30-45	22

Figure 3-4 AFM particle size distribution
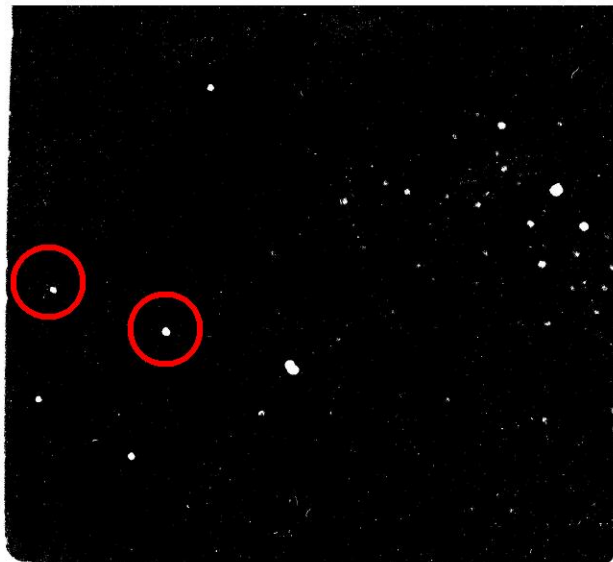
Figure 3-5 TEM image of gold nanoparticles

The reagent, 3-MPTMS, has three methoxy groups that interact with the silicon surface and a sulfur group that also reacts with gold nanoparticles. One drop of gold nanoparticle solution was placed on the silicon surface and analyzed using SEM/EDS (EMAX) for the surface analysis of gold nanoparticles. SEM/EDS provides chemical analysis of the field of view or spot analyses of nanoparticles. This instrument detects more than 90 elements. Figure 3-6 shows the result of the SEM/EDS analysis of a solution composed of isopropanol and BBI gold nanoparticles. The chemical composition of the gold nanoparticle surfaces consisted of 91.0 wt % Si, 8.10 wt % Au, and 0.90 wt % Sn. SEM/EDS indicated that BBI gold nanoparticles do not contain a sulfur component in the colloid solution. Figure 3-7 shows the SEM/EDS result where the solution analyzed was made with one drop of 3-MPTMS in the isopropanol and BBI gold nanoparticle solution. We found that 82.96 wt % Si, 16.02 wt % Au, and 1.02 wt % S were present. On the basis of these test results, we concluded that the unknown ligand of the BBI gold nanoparticle surface is chemically modified with the sulfur component of 3-MPTMS.

Spectrum processing :
No peaks omitted
Processing option : All elements analyzed (Normalised)
Number of iterations = 3
Standard :
Si   SiO2   1-Jun-1999 12:00 AM
Sn   Sn   1-Jun-1999 12:00 AM
Au   Au   1-Jun-1999 12:00 AM

Element	Weight%	Atomic%
Si K	91.00	98.52
Sn L	0.90	0.23
Au M	8.10	1.25
Totals	100.00	
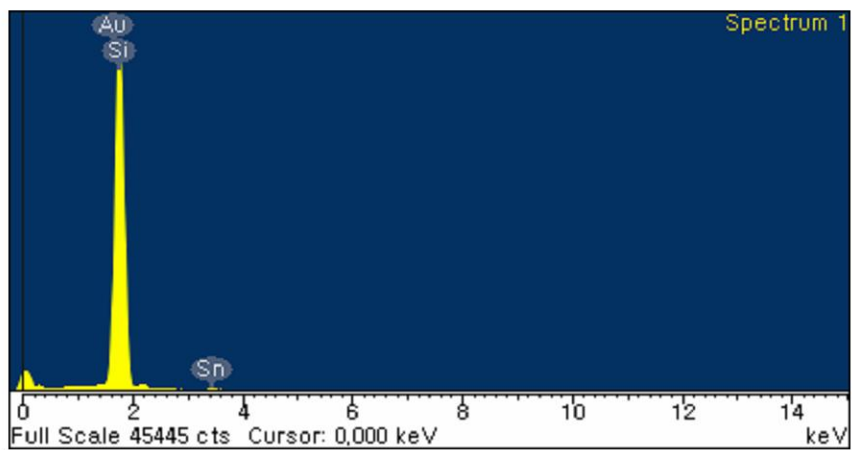
Figure 3-6 *SEM-EDS analysis (isopropanol and gold nanoparticle mixed solution)*
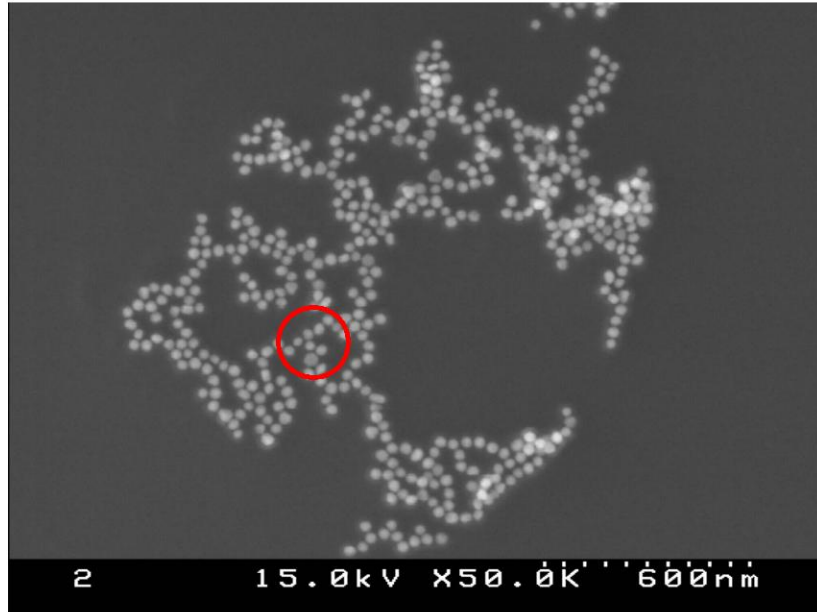
Spectrum processing :
Peak possibly omitted : 0.540 keV

Processing option : All elements analyzed (Normalised)
Number of iterations = 3

Standard :
Si   SiO2   1-Jun-1999 12:00 AM
S   FeS2   1-Jun-1999 12:00 AM
Au   Au   1-Jun-1999 12:00 AM

Element	Weight%	Atomic%
Si K	82.96	96.31
S K	1.02	1.04
Au M	16.02	2.65
Totals	100.00	
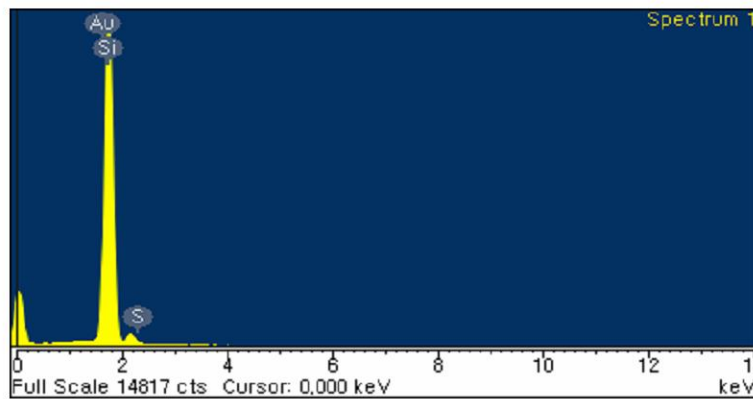
Figure 3-7 *A drop of 3-MPTMS into isopropanol and gold nanoparticle mixed solution*

56

It is important to control the number of gold nanoparticles to maximize the interactions with the silicon surface. We first increased the amount of the gold nanoparticle solution. We found that the density of gold nanoparticles deposited on the silicon surface depends upon the amount of the BBI gold nanoparticles solution. By increasing the concentration of the gold nanoparticle solution, we found a corresponding high concentration of gold nanoparticles on the silicon surface. AFM images in Figure 3-8 illustrate the increasing amount of BBI gold nanoparticles on a silicon surface.

(a)

57
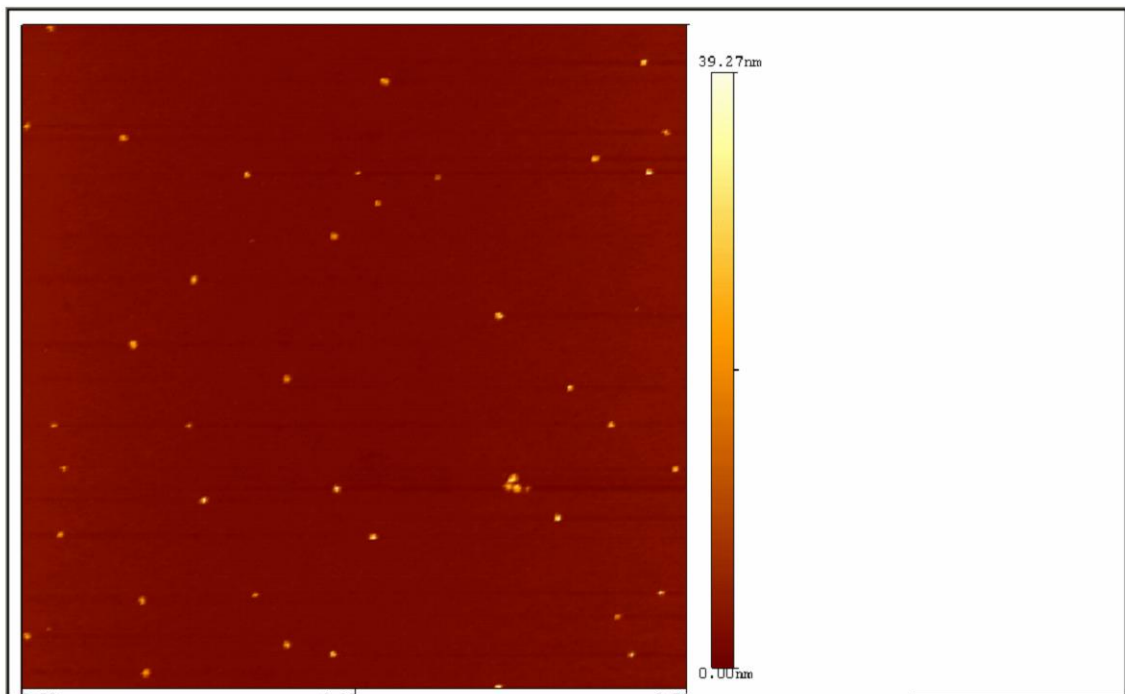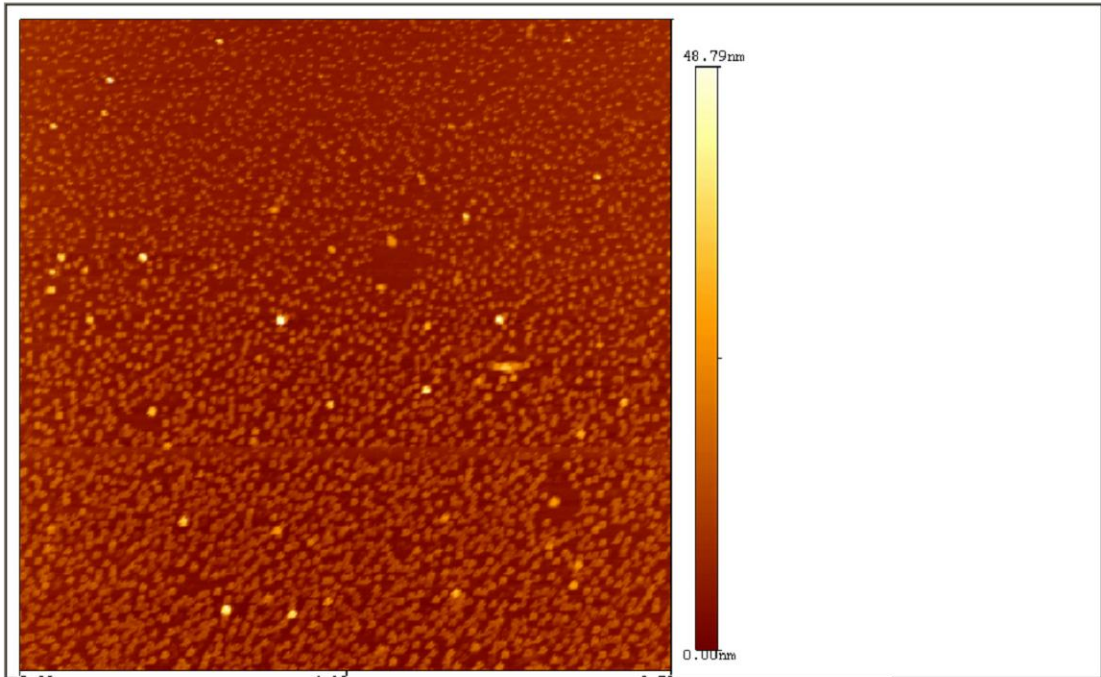
(b)
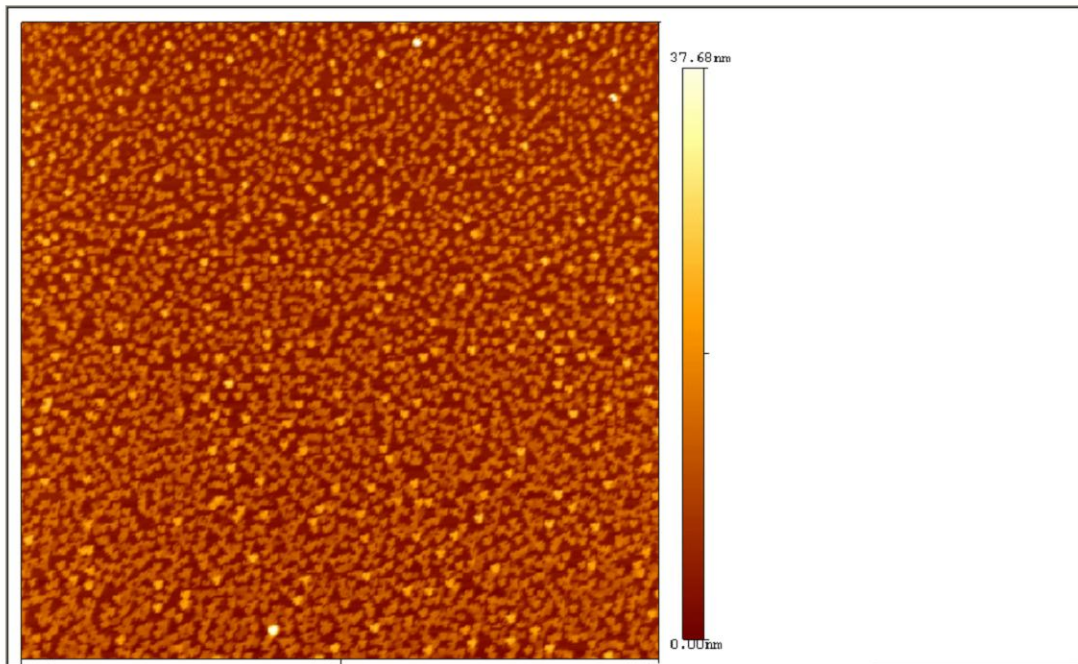
(c)

Figure 3-8 AFM image (9.78μm ×9.78μm) of gold nanoparticles

(1drop (a), 10drops (b), 20drops (c))

58

Second, silicon samples were immersed into gold nanoparticle solutions that consisted of 10 ml isopropanol, BBI gold nanoparticles (1 drop or 20 drops), and one drop of 3-MPTMS to examine the effect of deposition time, which was varied from 1 to 3 hour. The amount of BBI gold nanoparticles used were 1 drop (low final concentration) and 20 drops (high final concentration), respectively. Figure 3-9 shows the effect of deposition time effect in the case of a low final concentration (1 drop). AFM images show that a longer deposition time increased the surface coverage and the density of gold nanoparticles when a small amount of gold nanoparticles was used. However, under high amounts of gold nanoparticle solution (20 drops) the deposition of the gold nanoparticles was not improved by time. Figure 3-10 shows that the numbers of gold nanoparticles were similar in most cases with a tight coverage of gold nanoparticles. This suggests that the silicon surface and gold nanoparticles form a strong interaction in a short time. As a result, the functionalized silicon surface is quickly packed with thiol-coated gold nanoparticles.
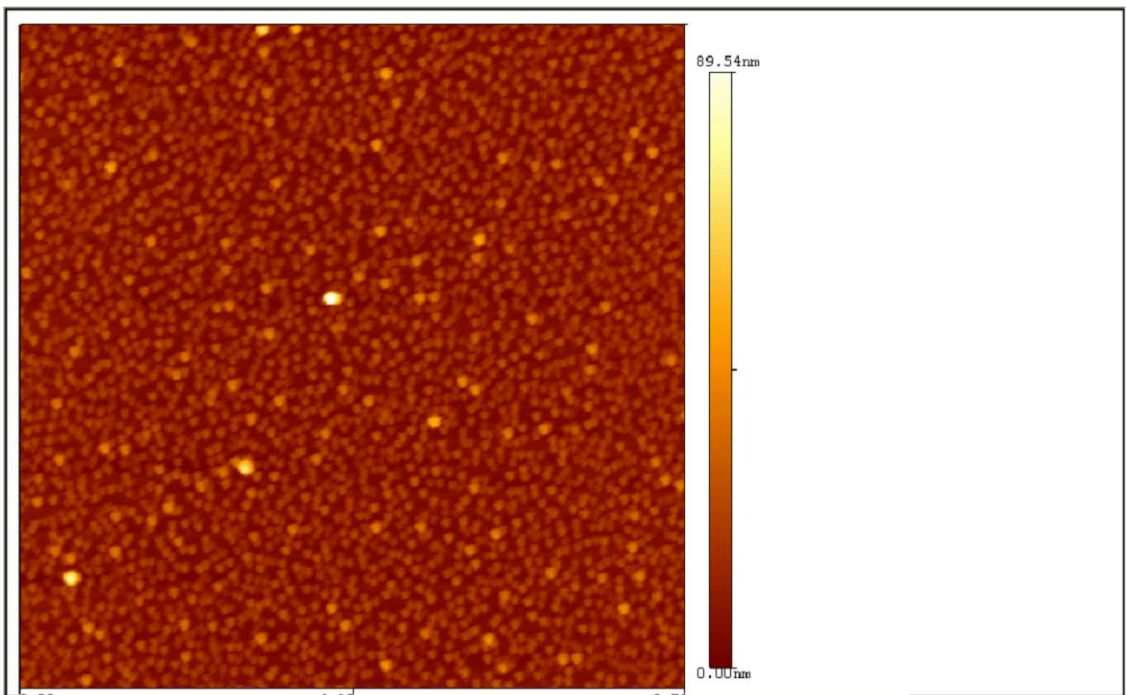
(a)

(b)

(c)

(d)

61
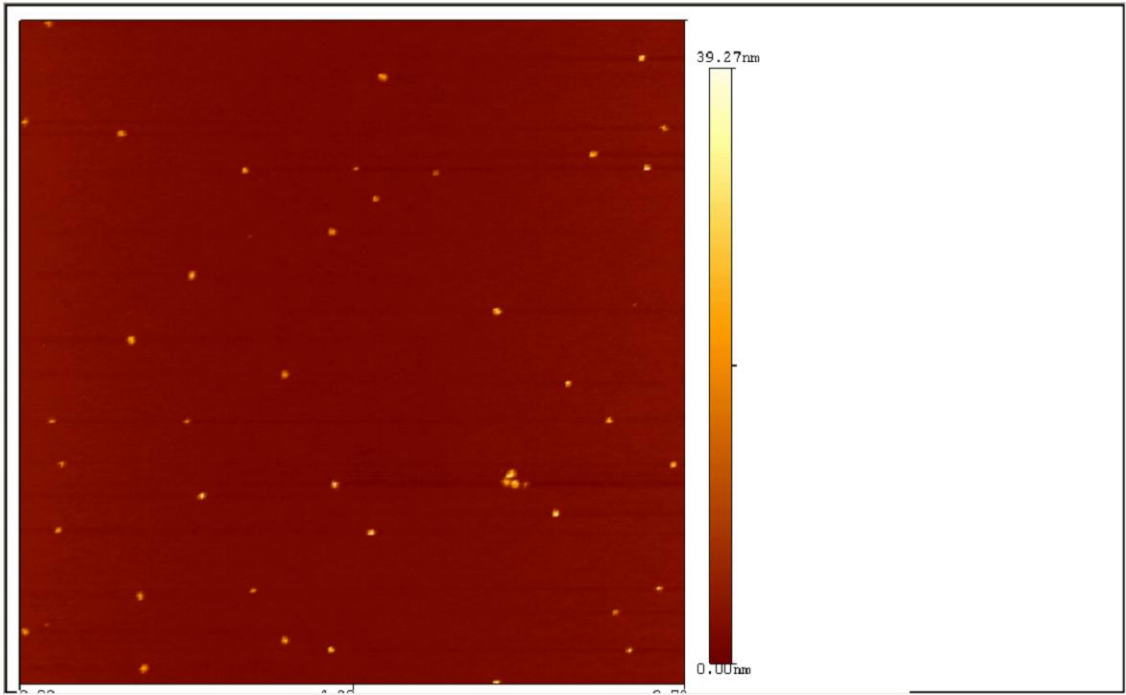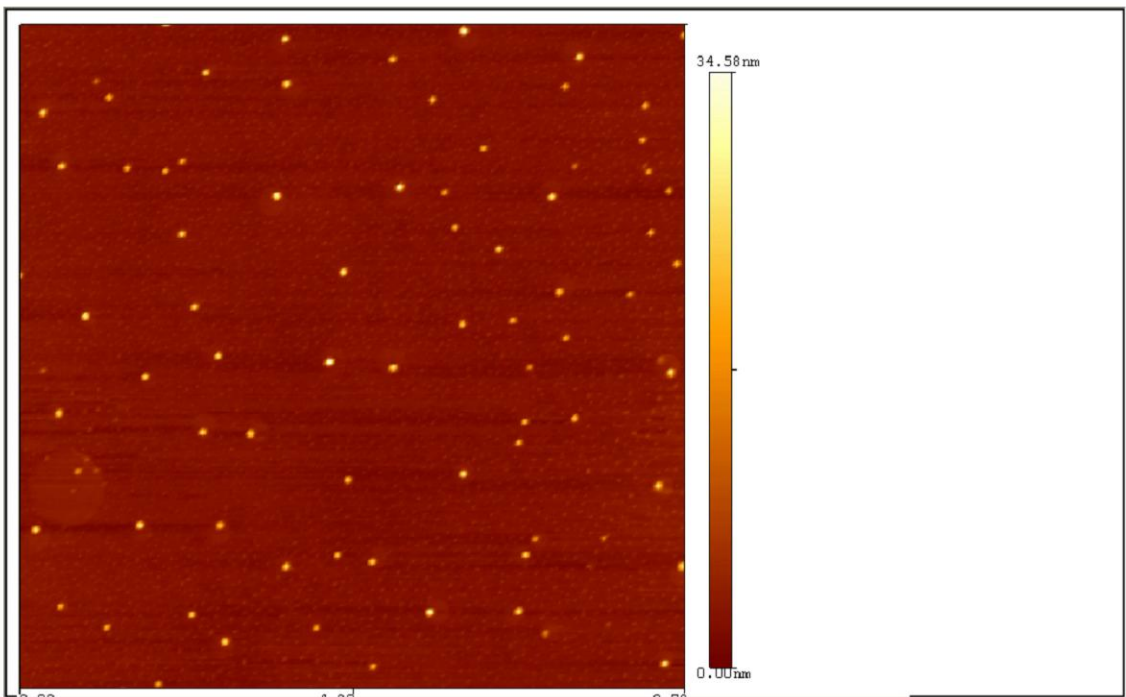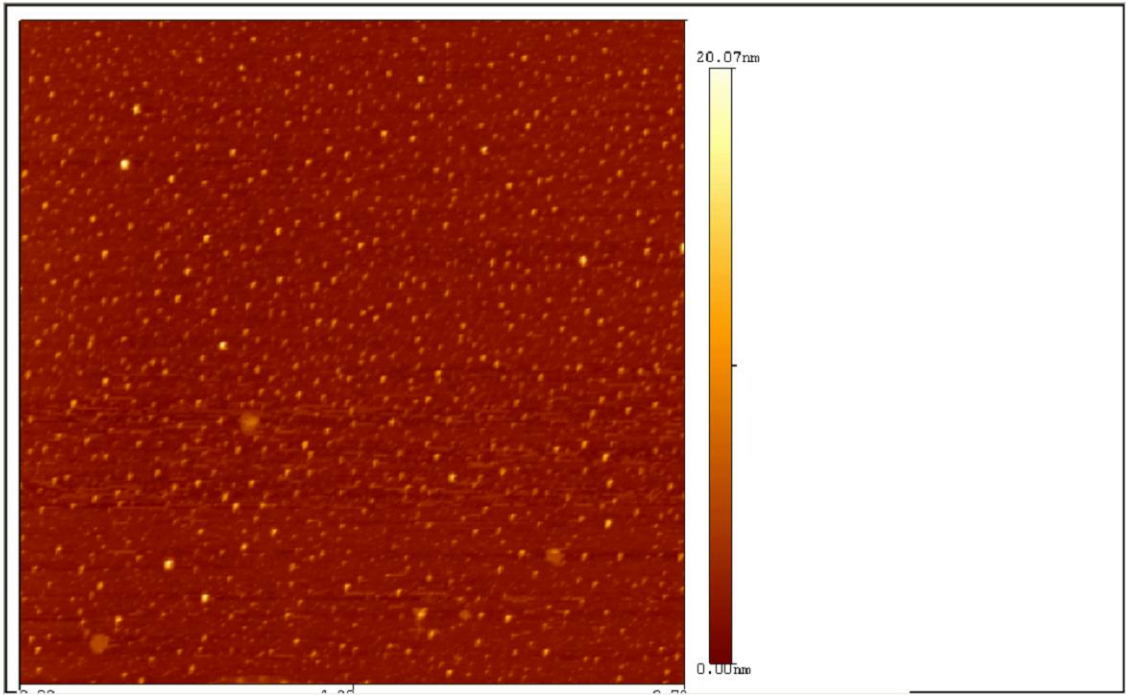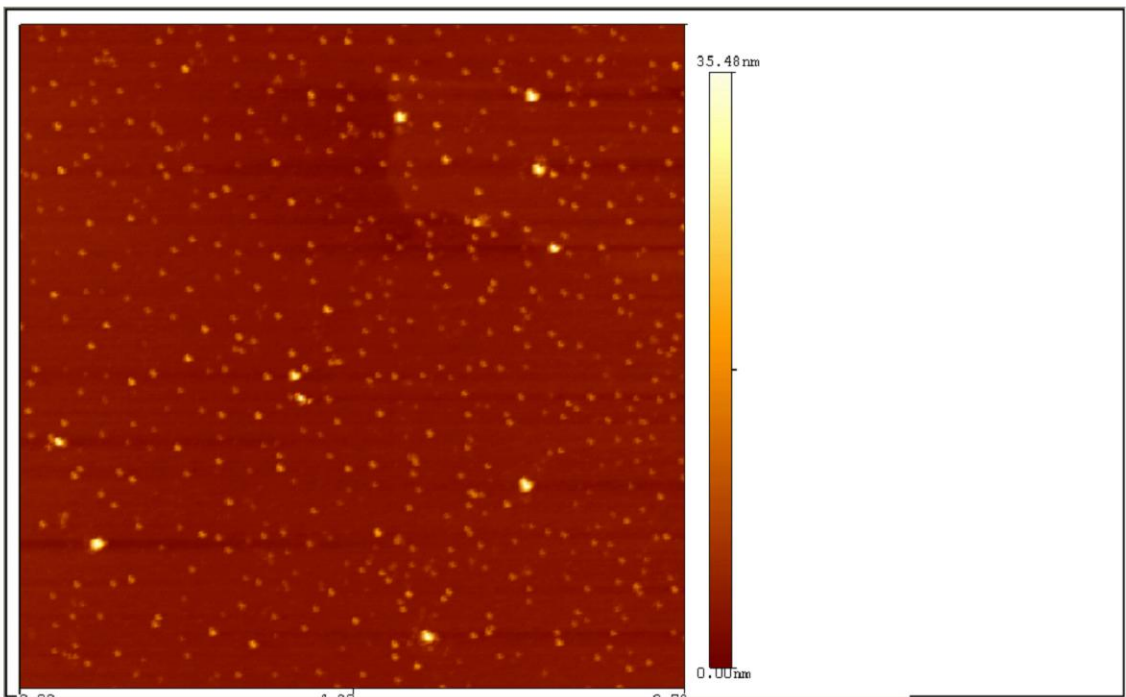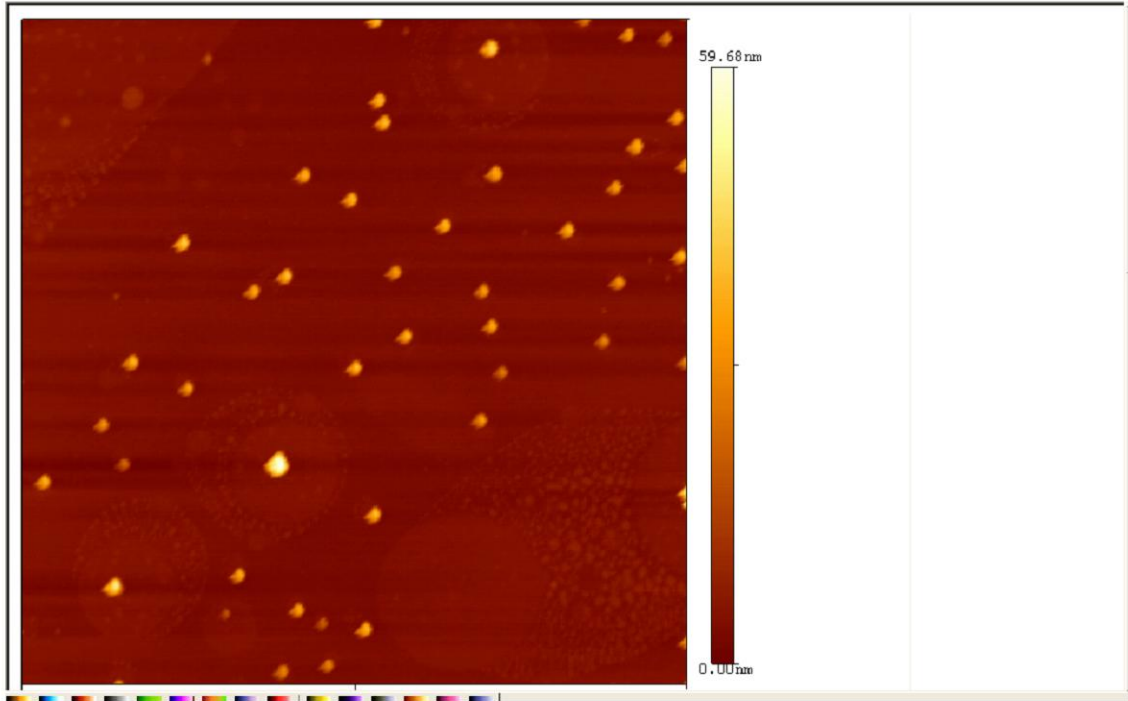
(e)

Figure 3-9 *Deposition time effect in case of low concentration (1 drop)*

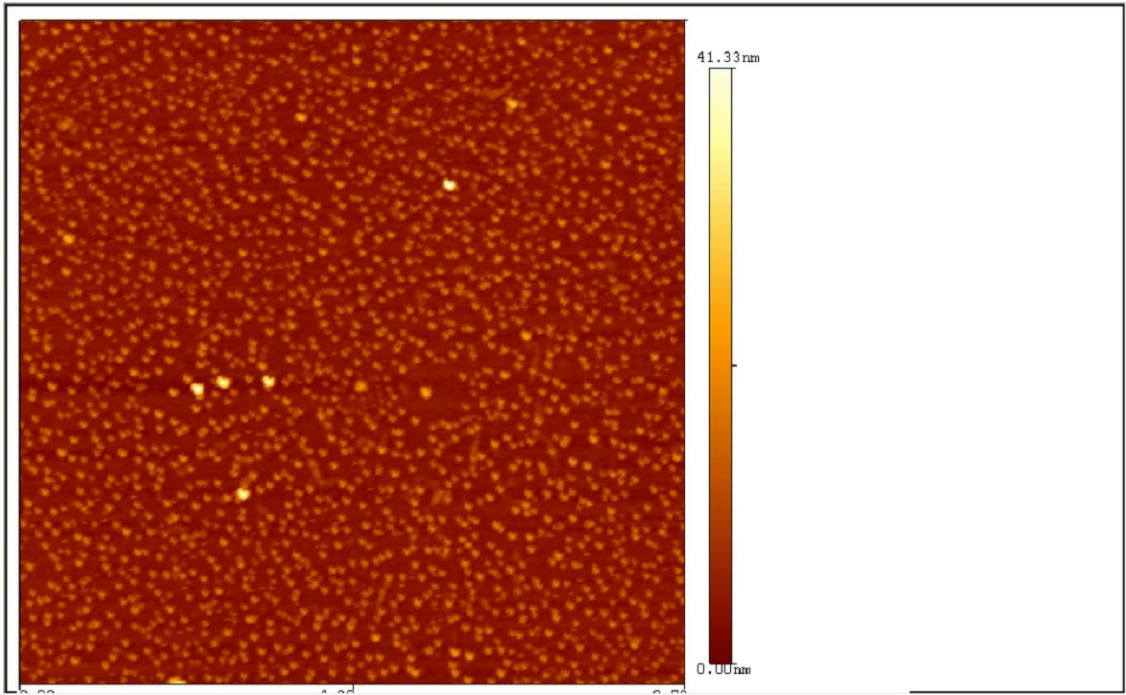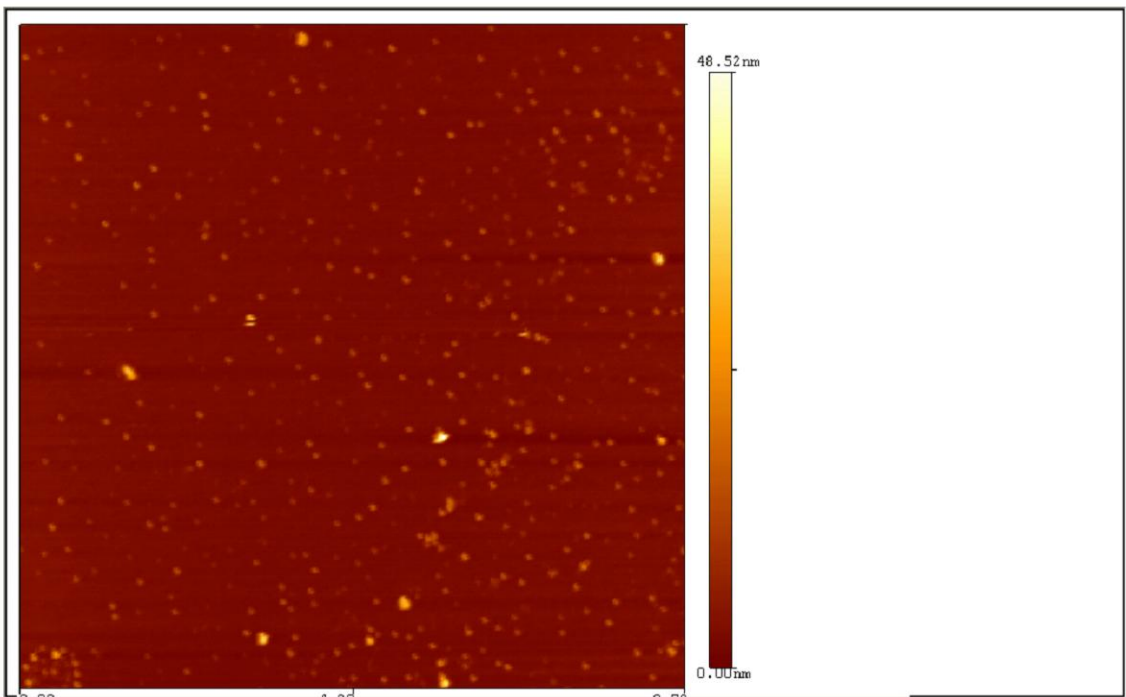*(1 hr(a), 2 hr(b), 3 hr(c), 4 hr(d), 5 hr(e))*
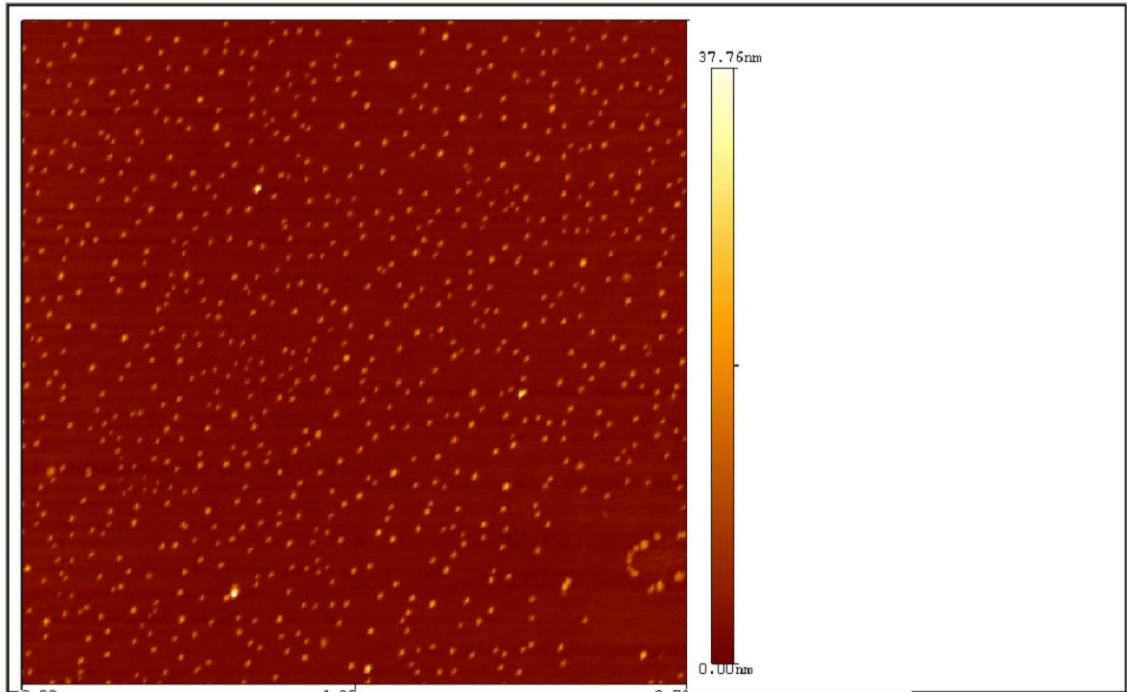
(a)

(b)

(c)

(d)

64
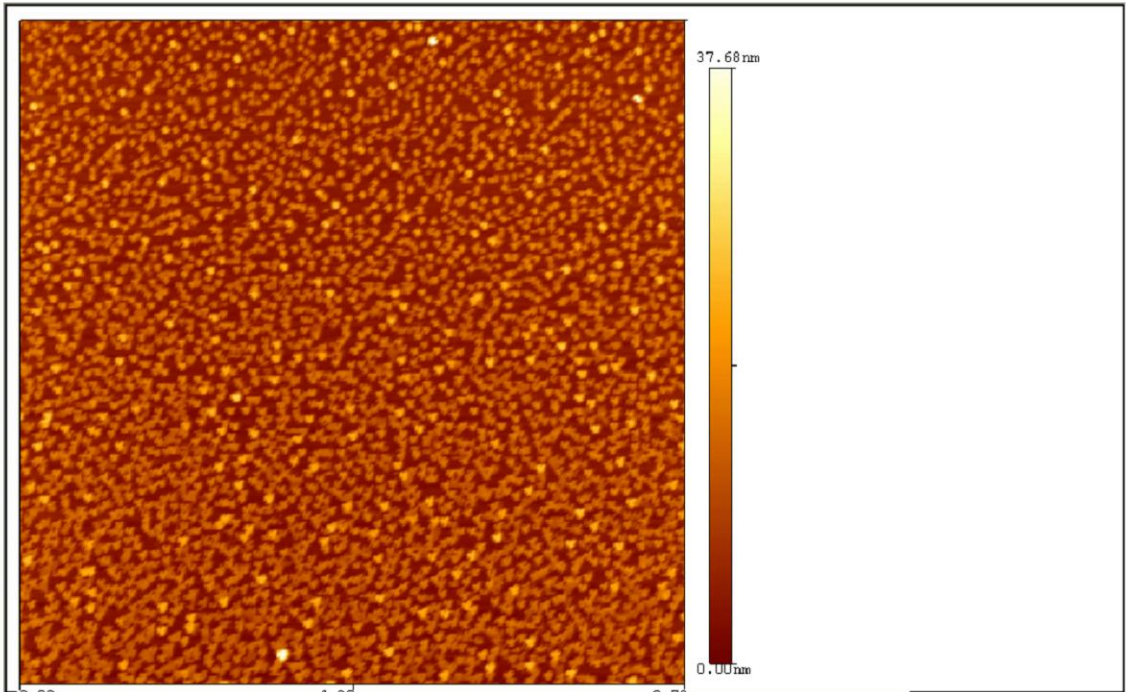
(e)

Figure 3-10 Deposition time effect in the case of high concentration (20 drops)

(1 hr(a), 2 hr(b), 3 hr(c), 4 hr(d), 5 hr(e))

Third, the density of the solution was examined by increasing the concentration of 3-MPTMS. Because 3-MPTMS has strong and fast interactions with the silicon surface, the surface becomes dirty with 3-MPTMS upon exposure for longer than 1 hour. Therefore, 1 hour is the best condition for the density control. Figure 3-11 shows the density control of gold nanoparticles with 3-MPTMS on the silicon surface. It demonstrates that as the amount of 3-MPTMS increases, the numbers of gold nanoparticles also increased. However, higher concentrations of 3-MTPMS (> 7 drops) produced big clusters on the surface making it impossible to perform particle analysis with AFM.
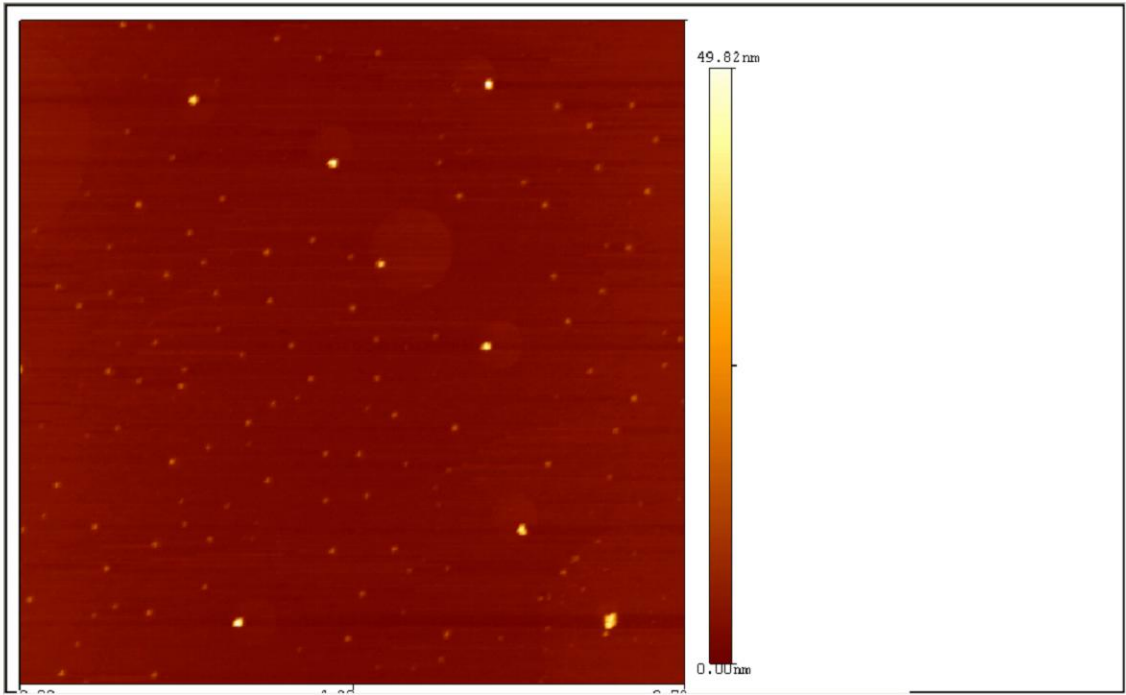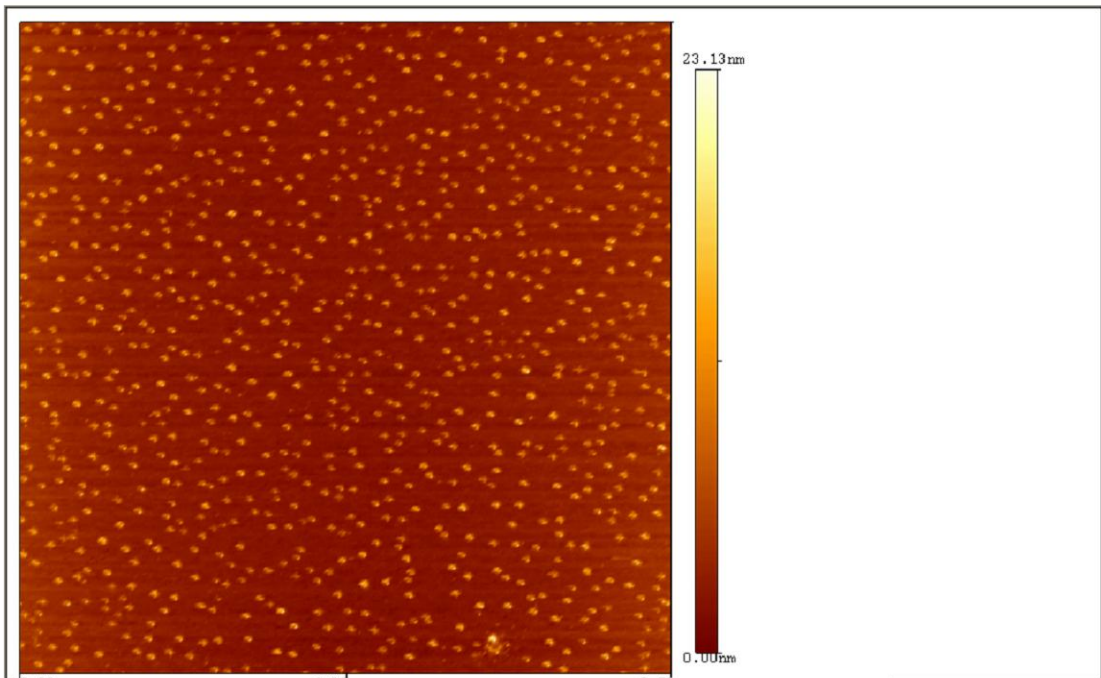
(a)
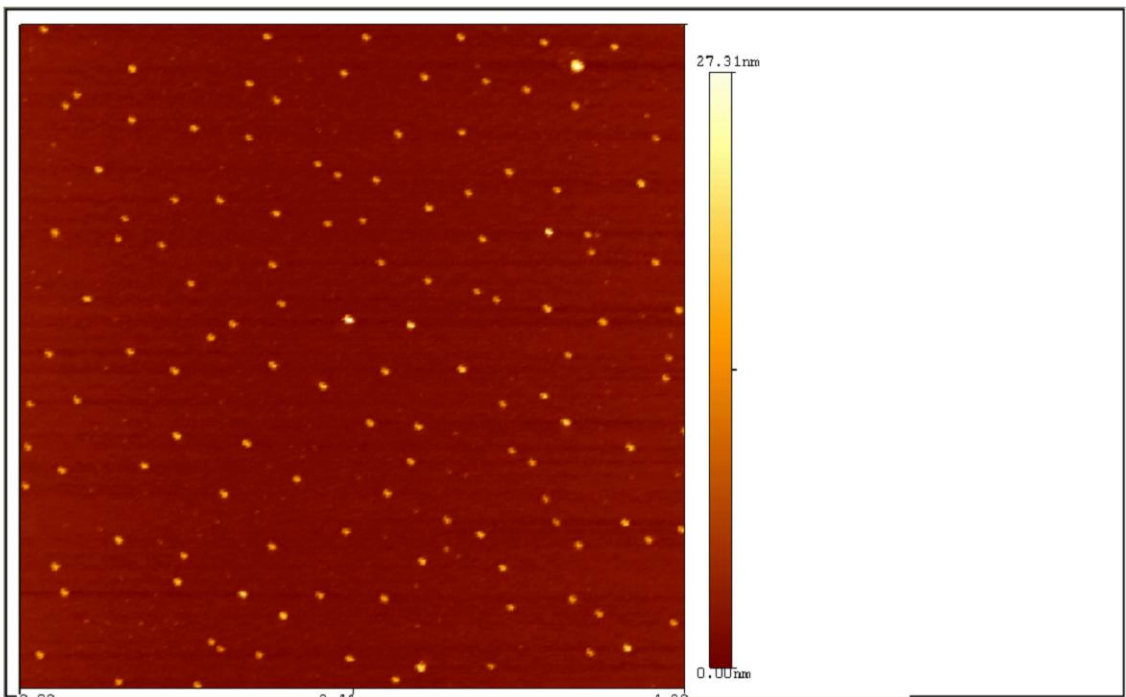
(b)
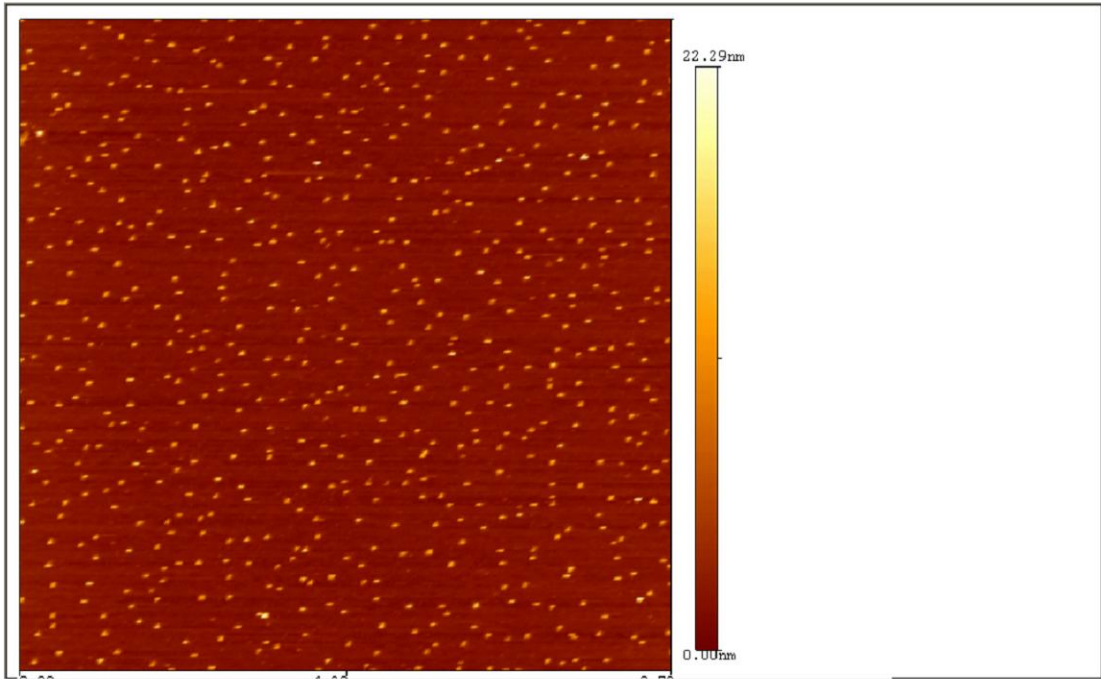
(c)

(d)

Figure 3-11 *3-MPTMS effects in the density control*

(1 drop (a), 3 drops (b),5 drops (c), 7 drops (d))

Finally, the effect of temperature on gold nanoparticle deposition on a silicon surface was tested. Figure 3-12 shows gold nanoparticle density on a silicon surface. A non-thermal silicon surface and a thermal silicon sample had similar numbers of gold nanoparticles under the same conditions. This suggests that temperature did not play an important role in the deposition of gold nanoparticles on the silicon surface.
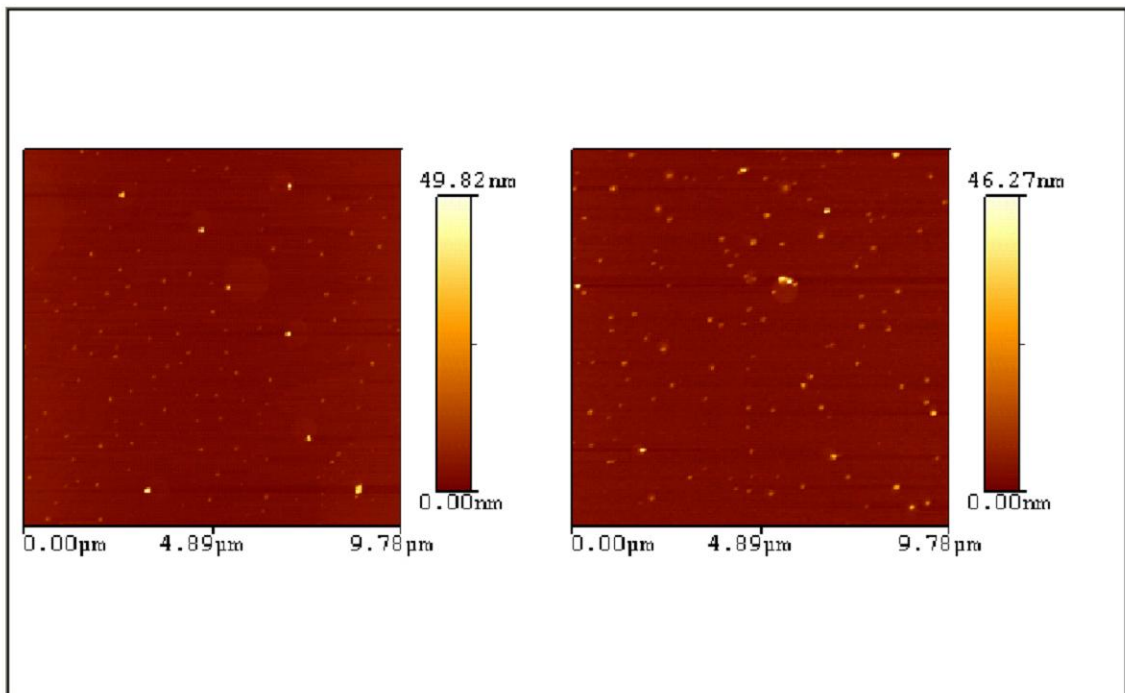

Figure 3-12 *AFM image of thermal Effect*

(No heat-left side, Heat-right side)

Overall, we tested 3-MPTMS modified silicon surfaces loaded with functionalised gold nanoparticles. Various conditions like the concentration of gold nanoparticles, deposition time, and 3-MPTMS concentrations contribute to the increase in particle density as shown in our AFM images (Fig. 3-13 to Fig. 3-16). These results were

obtained using the particle analysis tool from the AFM instrument, and can be used to

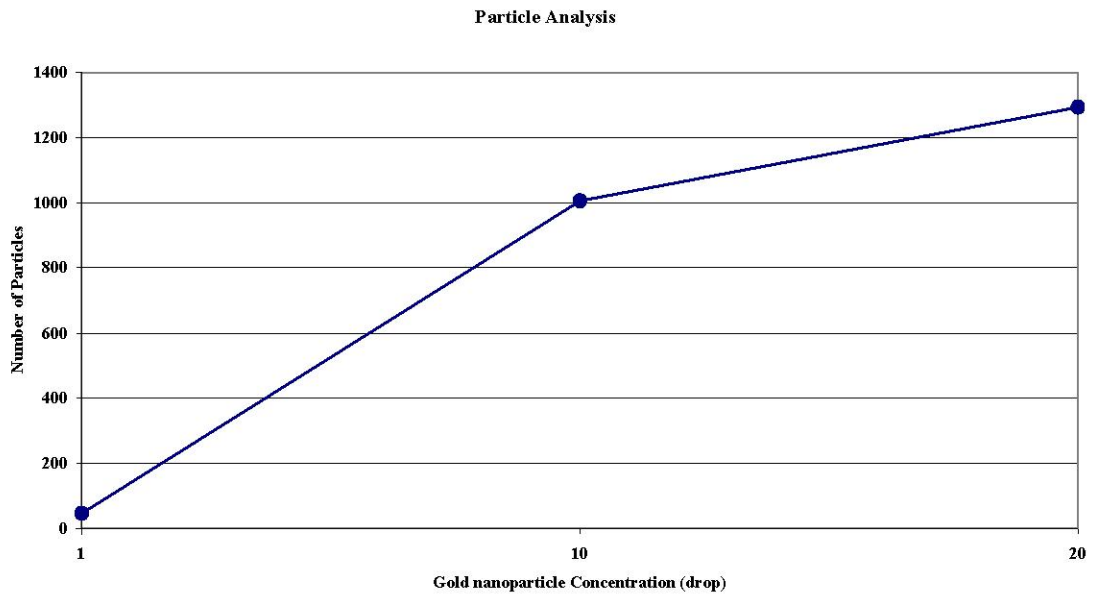predict the particle density under any condition.

Figure 3-13 *Analysis of gold nanoparticle concentration effect from Figure 3-8*
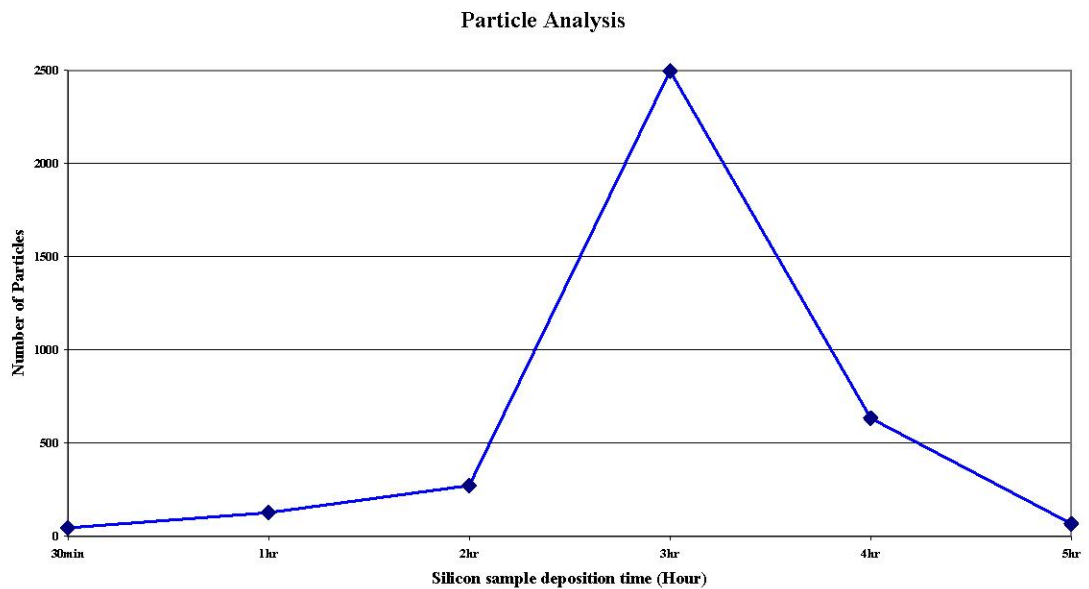
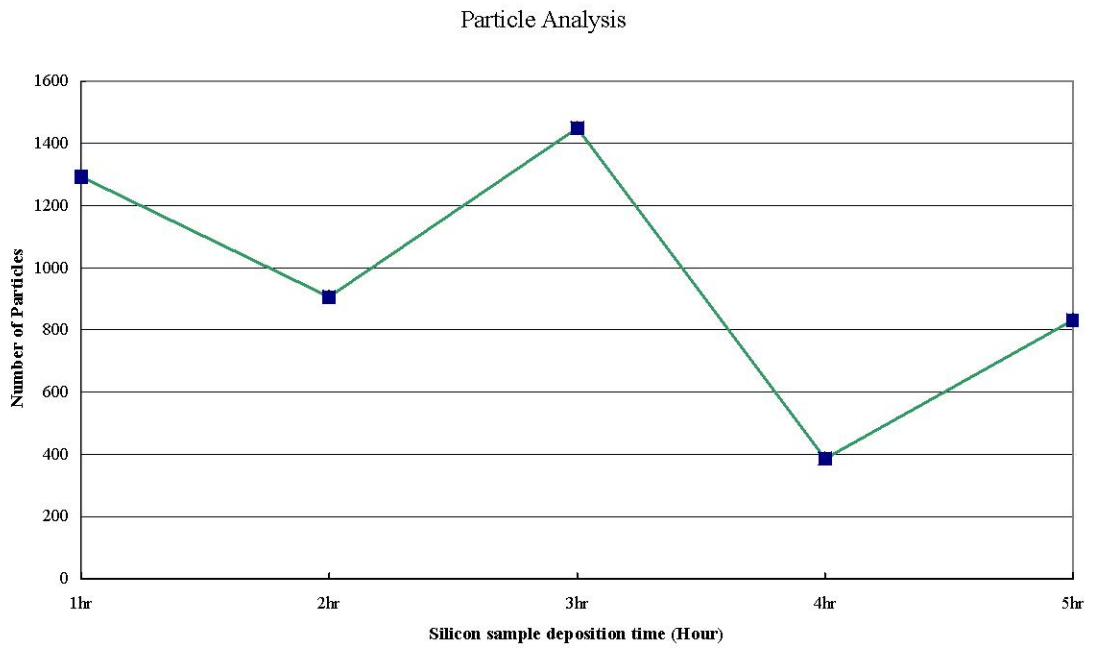**Figure 3-14** *Analysis of deposition time effect in low concentration from Fig. 3-9*

69

Particle Analysis

Figure 3-15 *Analysis of deposition time effect in high concentration from Fig. 3-10*
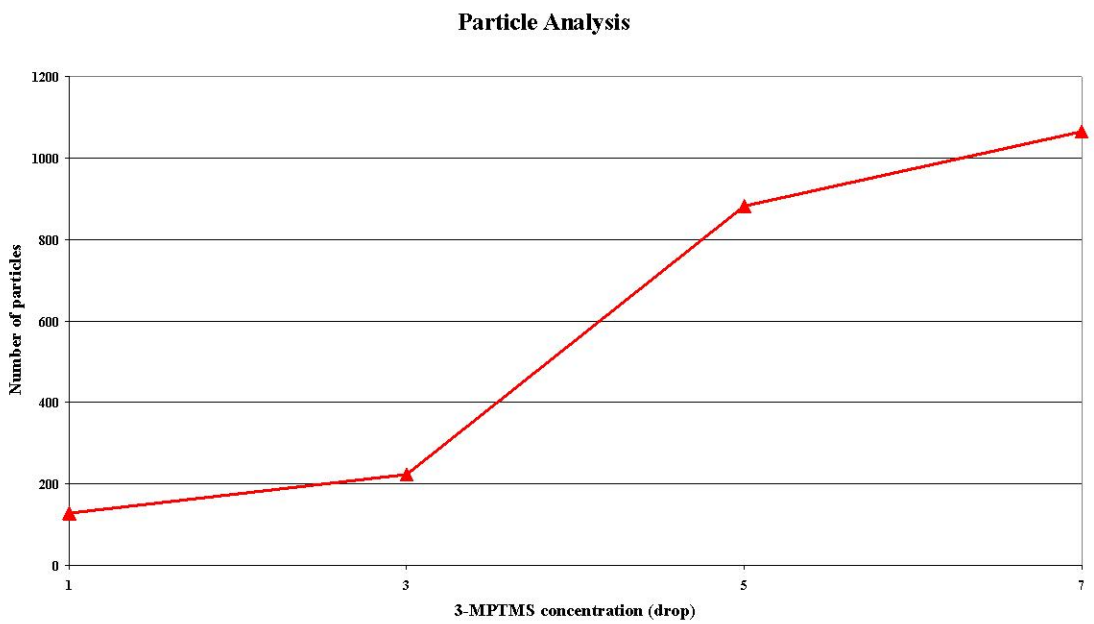
Particle Analysis

Figure 3-16 *Analysis of 3-MPTMS effect from Fig. 3-11*

70

3.4 Conclusions

A uniform distribution of BBI gold nanoparticles on silicon wafers can be obtained by using thiolate-coated gold nanoparticles and a 3-MPTMS modified silicon surface. We report how the silicon surface and the BBI gold nanoparticle surface are modified by 3-MPTMS and how the density of gold nanoparticles is controlled by several factors. The density of gold nanoparticles is influenced by the concentration of BBI gold nanoparticles, the deposition time, and 3-MPTMS concentrations.

However, the concentration of gold nanoparticles does not influence the deposition time in high concentration. This is because silicon surfaces functionalized by 3-MPTMS react with gold nanoparticles over a short period of time. Also, a high concentration of 3-MPTMS prevents deposition of gold nanoparticles on the silicon surface.

3.5 References

[1] T. Cui, F. Hua, Y. Lvov, "Lithographic approach to pattern multiple nanoparticle thin films prepared by layer-by-layer self-assembly for microsystems", *Sensor and Actuators A*, 114, 501-504 (2004)

[2] S. Ingvarsson, O. D. Jonsson, E. H. Huijbens, *Magnetic nanoparticles in composite materials and devices*, 1st Edn, The University of Iceland Press, Reykjavik, Iceland (2005)

[3] C. Minard-Basquin, R. Kugler, N. N. Matsuzawa, A. Yasuda, "Gold-nanoparticle-assisted oligonucleotide immobilization for improved DNA detection", *IEE Proc. Nanobiotechnology*, 152, 97-103 (2005)

[4] T. Liu, J. Tang, L. Jiang, "The enhancement effect of gold nanoparticles as a surface modifier on DNA sensor sensitivity," *Biochemical and Biophysical Research Communications*, 313, 3-7 (2004)

[5] S. Lan, M. Veiseh, M. Zhang, "Surface modification of silicon and gold-patterned silicon surfaces for improved biocompatibility and cell patterning selectivity", *Biosensors and Bioelectronics*, 20, 1697-1708 (2005)

[6] M. C. Daniel, D. Astruc, "Gold nanoparticles: Assembly, supramolecular Chemistry, Quantum-size-related Properties, and Applications toward biology, catalysis, and nanotechnology", *Chem. Rev.*, 104, 293-346 (2004)

[7] X. Ling, X. Zhu, J. Zhang, T. Zhu, M. Liu, L. Tong, Z. Liu, "Reproducible Patterning of Single Au Nanoparticles on Silicon Substrates by Scanning Probe Oxidation and Self-Assembly", *J. Phys. Chem. B*, 109, 2657-2665 (2005)

[8] C. Ritter, M. Heyde, B. Stegemann, K. Rademann, "Contact-area dependence of frictional forces: Moving adsorbed antimony nanoparticles", *Phys. Rev. B*, 71, 085405-1-085405-7 (2005)

[9] F. W. DelRio, M. L. Dunn, B. L. Boyce, A. D. Corwin, M. P. de Boer. "The effect of nanoparticles on rough surface adhesion", *J. Appl. Phys.*, 99, 104304-104312 (2006)

[10] C. Jiang, S. Markutsya, V. V. Tsukruk, "Tuning optical response of polymer-nanoparticle layered films," *Polymer Materials: Science and Engineering*, 89, 346- , (2003)

[11] D. S Tsai, C. H. Chen, C. C. Chou, "Preparation and characterization of gold-coated silver triangular platelets in nanometer scale", *Materials Chemistry and Physics*, 90, 361-366 (2005)

[12] B.G. Prevo, J.C. Fuller, O. D. Velev, "Rapid Deposition of Gold Nanoparticle Films with Controlled Thickness and Structure by Convective Assembly", *Chem. Mater.*, 17, 28-35 (2005)

[13] J. H. Kim, S. H. Ehrman, G. W. Mulholland, T. A. Germer, "Polarized light scattering from metallic particles on silicon wafers", *Proc.SPIE*, 4449, 281-290 (2001)

[14] Y. Ma, N. Li, C. Yang, X. Yang, "One-step synthesis of amino-dextran-protected gold and silver nanoparticles and its application in biosensor", *Anal Bioanal Chem*, 382, 1044-1048 (2005)

[15] G. Schmid, U. Simon, "Gold nanoparticles: assembly and electrical properties in 1-3 dimensions", *Chem. Commun.*, 6, 697-710 (2005)

[16] H. Zhu, Z. Pan, E. W. Hagaman, C. Liang, S. H. Overbury, S. Dai, "Facile one-pot synthesis of gold nanoparticles stabilized with bifunctional amino/siloxy ligands", *Journal of Colloid and Interface Science*, <u>287</u>, 360-365 (2005)

[17] Y. Huh, M. L. H. Green, Y. H. Kim, J. Y. Lee, C. J. Lee, "Control of carbon nanotube growth using cobalt nanoparticles as catalyst", *Applied Surface Science*, <u>249</u>, 145-150 (2005)

[18] A. Csaki, P. Kaplanek, R. Moller, W. Fritzsche, "The optical detection of individual DNA-conjugated gold nanoparticles labels after metal enhancement", *Nanotechnology*, <u>14</u>, 1262-1268 (2003)

[19] K. C. Grabar, P. C. Smith, M. D. Musick, J. A. Davis, D. G. Walter, M. A. Jackson, A. P. Guthrie, M. J. Natan, "Kinetic Control of Interparticle Spacing in Au colloid-Based Surfaces: Rational Nanometer-Scale Architecture", *J. Am. Chem. Soc.,* <u>118</u>, 1148-1153 (1996)

[20] H. C. Choi, S. Kundaria, D. Wang, A. Ajavey, Q. Wang, M. Rolandi, H. Dai, "Efficient formation of iron nanoparticle catalysts on silicon oxide by hydroxylmaine for carbon nanotube synthesis and electronics" *Nano letters*, <u>3</u>, 157-161 (2003)

[21] L. Maya, K. A. Stevenson, G. Muralidharan, T. G. Thundat, E. A. Kenik, "Assembly of Nanocluster on Silicon Surfaces", *Langmuir*, <u>18</u>, 2392 -2397 (2002)

[22] H. Hirano, K. Sato, T. Osaka, H. Kuniyasu, T. Hattori, "Damage-Free Ultradiluted HF/Nitrogen Jet Spray Cleaning for Particle Removal with Minimal Silicon and Oxide Loss", *Electrochem. Solid-State Letters*, <u>9</u>, G62-G65 (2006)

[23] R. Vos, M. Lux, K. Xu, W. Fyen, C. Kenens, T. Conard, P. Mertens, M. Heyns, Z. Hatcher, M. Hoffman, "Removal of Submicrometer Particles from Silicon Wafer

Surfaces Using HF-Based Cleaning Mixtures", *Journal of Electrochem. Soc.*, <u>148</u>, G683-G691 (2001)

[24] A. P. Chuklanov, S. A. Ziganshina, A. A. Bukharaev, "Computer program for the grain analysis of AFM images of nanoparticles placed on a rough surface", *Surface and Interface Analysis*, <u>38</u>, 679-681 (2006)

[25] Y. Wang, S. Han, A. L. Briseno, R. J. G. Sanedrin, F. Zhou, "A modified nanosphere lithography for the fabrication of aminosilane/polystyrene nanoring arrays and subsequent attachment of gold or DNA-capped gold nanoparticles", *J. Mater. Chem.*, <u>14</u>, 1-8 (2004)

[26] R. Lenigk, M. Carles, N. Y. Ip, N. J. Sucher, "Surface Characterization of a Silicon-Chip-Based DNA Microarray," *Langmuir*, <u>17</u>, 2497-2501 (2001)

[27] H. J. Kang, F. D. Blum, "Structure and dynamics of amino functional silanes adsorbed on silica surface", *J. Phys. Chem.*, <u>95</u>, 9391-9396 (1991)

[28] R. J. Markovich, X. Qiu, D. E. Nichols, C. Pidgeon, " Silica substrate amine effect on the chemical stability and chromatographic properties of end-capped immobilized artificial membrane surface", *Anal. Chem.*, <u>63</u>, 1851-1860 (1991)

[29] K. C. Popat, R. W. Johnson, T. A. Desai, "Characterization of vapor deposited thin silane films on silicon substrates for biomedical microdevices", *Surface and Coating Technology*, <u>154</u>, 253-261 (2002)

[30] R. D. Tilley, S. Saito, "Preparation of large scale monolayer of gold nanoparticles on modified silicon substrates using a controlled pulling method", *Langmuir*, <u>19</u>, 5115-5120 (2003)